The Innate Immune Response to Invasive Pulmonary Aspergillosis: A Systems Modeling Approach

Henrique AL Ribeiro[1], Luis Sordo Vieira[1,2], Yogesh Scindia[1], Bandita Adhikari[3], Matthew Wheeler [1], Adam Knapp[1], William Schroeder[4], Borna Mehrad[1], Reinhard Laubenbacher[1*]

1 Division of Pulmonary, Critical Care, and Sleep Medicine, University of Florida, Gainesville, FL, USA
2 Department of Psychiatry, University of Florida, Gainesville, FL, USA
3 Center for Quantitative Medicine, School of Medicine, University of Connecticut, Farmington, CT, USA
4 Kitware Inc., Clifton Park, NY, USA

* reinhard.laubenbacher@medicine.ufl.edu

Abstract

Invasive aspergillosis is a fungal respiratory infection that poses an increasingly serious health risk with the rise in the number of immunocompromised patients and the emergence of fungal strains resistant to first-line anti-fungal drugs. Consequently, there is a pressing need for host-centric therapeutics for this infection, which motivated the work presented in this paper. Given the multi-scale nature of the immune response, computational models are a key technology for capturing the dynamics of the battle between the pathogen and the immune system. We describe such a multi-scale computational model, focused on the mechanisms for iron regulation, a key element for fungal virulence in the pathogen *Aspergillus fumigatus*. A key feature of the model is that its parameters have been derived from an extensive literature search rather than data fitting. The model is shown to reproduce a wide range of published time course data, as well as custom validation data generated for this purpose. It also accurately reproduces many qualitative features of the initial course of infection.

Author summary

The battle between the immune system and invading pathogens is highly dynamic, involving mechanisms from the intracellular and tissue scales to the whole-body scale. Medical interventions aim to change the dynamic trajectory of the infection in the patient's favor. Computational models that capture the system dynamics can play an important role in understanding the mechanisms determining the course of infection and discovering possible interventions. The model described here focuses on a well-defined and complex mechanism, the "battle over iron" between the host and a respiratory fungal pathogen, a crucial virulence factor. It includes several cell types, cytokines, and other molecules involved in the immune response. A key feature of the model is its broad validity, resulting from efforts to find information about numerical values for all of the many model parameters in the literature, rather than determining them by fitting the model to one or more time courses of experimental data. Consequently, the model can form the basis for investigating host-centric interventions in the course of the disease, as well as for expanding it to study other pathogens and inflammatory lung diseases.

Introduction

Invasive aspergillosis is a human infection with increasing incidence, related to the use of immunosuppressive therapies, such as cancer chemotherapy and immunosuppression for stem cell or solid organ transplantation [1]. More recently, it has also been observed that 19.6% to 33.3% of patients with COVID-19 in ICU were reported to have aspergillosis, mainly *A. fumigatus* [2]. Mortality remains high, 30-60% in recent surveys [3], despite advances in diagnostics and therapy. Increasing triazole resistance in this infection [4] has raised the specter of a "perfect storm" [5] in an increasing population of susceptible individuals with a diminished repertoire of treatment options.

The research presented here was motivated by the search for host-centric interventions in immuno-compromised patients that can be used in combination with antifungal treatments. An important mechanism in innate immunity is the sequestration of iron from pathogens, a nutrient critical for nearly all organisms. A well-established literature supports the concept that the "battle over iron" is characteristic of the host's attempt to attenuate microbial growth during many infections [6]. Iron is particularly relevant to the pathogenesis of aspergillosis [7]. The iron sequestration feature of the innate immune response involves several intertwined processes that unfold across spatial and temporal scales. This makes it challenging to assess the effect of perturbations of individual mechanisms on infection dynamics. A computational model that captures the key mechanisms, broadly reflects the underlying immune biology, and is well-validated, can play an essential role in hypothesis generation and the discovery of emergent properties of the immune response.

Several models related to respiratory *Aspergillus* infections and their pathology have been previously published. For example, agent-based models have shown the necessity of chemotactic signals for proper fungal clearance [8,9]. Our own work includes a model of the innate immune response to *A. fumigatus*, showing that a key determinant of infection is the range at which macrophages can detect the fungus [10], and an intracellular regulatory network linking iron metabolism to oxidative stress in a fungal cell [11]. The model is parametrized entirely with information from the literature, rather than through data fitting, and is validated by showing that it can recapitulate a wide range of experimental data reported in the literature that were not used in its construction, as well as experimental data generated for this purpose. An extensive and detailed sensitivity analysis of model parameters was performed to identify key mechanisms that control the pathogenesis of the infection.

Materials and methods

A computational model of invasive aspergillosis

The model is an agent-based model of invasive pulmonary aspergillosis scaled to a mouse lung, the experimental system used in this study, focusing on the "battle over iron" between host and fungus. It integrates the critical players in the early immune response and the known mechanisms that govern their behavior and interactions, and is divided into seven conceptual components: space and time, molecules, cells, interactions between different cells and cells and molecules, movement, recruitment, and iron metabolism, as briefly described here.

Space and time

A three-dimensional space representing a small portion of a mouse lung is divided into a discrete grid of one thousand voxels (10 voxels in each of 3 dimensions), representing a total volume of 6.4×10^{-2} μL. Each voxel has an edge length of 40 μm ($6.4 \times 10^{-5} \mu L$).

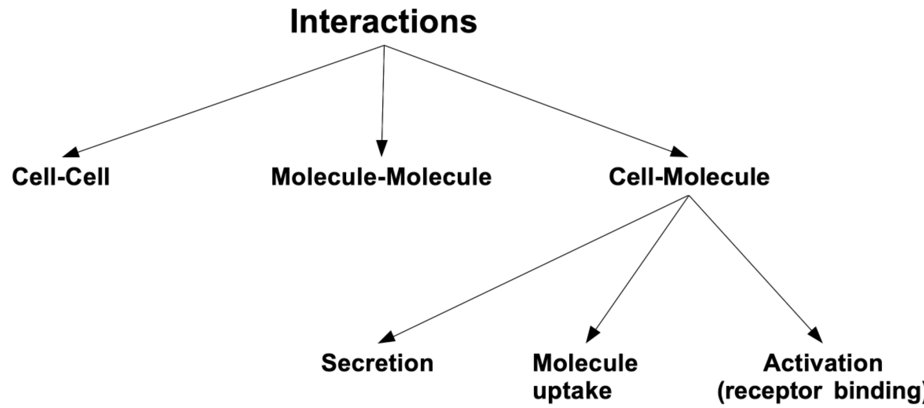

Fig 1. Figure showing the three general types of interactions: cell-cell, molecule-molecule, and cell-molecule. There are three kinds of cell-molecule interactions in turn: secretion (secretion is considered an interaction), molecule uptake, and activation (receptor activation). Receptor activation consists of a molecule activating a cell receptor, thereby changing the cell's internal state.

Cells and molecules have no space coordinate other than the voxel in which they are located at a given time. This approach is similar to that used in the general immune modeling platform C-IMMSIM [12]. The space has periodic boundary conditions, and simulated time progresses in discrete steps of two minutes.

Interactions

The interactions between different cells and molecules in the infection process comprise one of the model's critical aspects. They are divided into three types: molecule-molecule, cell-molecule, and cell-cell. Cell-molecule interactions, in turn, can be further divided into three types. Figure 1 depicts the interaction hierarchy.

An interaction between two cells of any type can only happen if the cells are located in the same voxel. These interactions are probabilistic events that lead to a possible change in internal states of both cells involved in the interaction. A molecular species is represented by a state variable that takes on continuous values (concentrations) and can interact with other model entities, either cells or molecules, in all voxels.

Cell-molecule interactions can consist of either secretion of the molecule by the cell, uptake of the molecule by the cell, or activation of a receptor on the cell surface. Receptor activation is a probabilistic event that can lead to a change of the internal state of the cell. The higher the concentration of the molecule in the voxel that a cell is located in the more likely it is to "activate" the cell.

Finally, molecule-molecule interactions comprise reactions between molecules, and these are modeled with Michaelian kinetics (Equation 1). Upon reaction, the reactants (S1 and S2) are consumed, and the product is formed. The parameter K_{cat} is forced to be equal to 1; this way, one avoids the reaction rate to be larger than the reactants' concentration:

$$v = \frac{K_{cat} \times S1 \times S2}{K_M + S1} \tag{1}$$

Molecules

The model includes sixteen different molecular species: TNF, IL-6, IL-10, CCL4, CXCL2, TGF-β, hepcidin, Tf (transferrin), $TfFe$ (transferrin bound to one iron atom), $TfFe_2$ (transferrin bound to two iron atoms), Lf (lactoferrin), $LfFe$ (lactoferrin bound to one iron atom), $LfFe_2$ (Lactoferrin bound to two iron atoms), TAFC (triacetylfusarinine C), TAFCBI (triacetylfusarinine C bound to iron), and iron. To reproduce an experiment with anti-TNF, the anti-TNF antibody is also included. Iron (free iron) acts as a temporary buffer for the transference between cells and carrier molecules (i.e., transferrin, lactoferrin, and siderophore - TAFC). In other words, iron is always bound to a carrier in this model.

For each molecule, the model has a *local* concentration, referring to a given voxel, a *global* one, referring to the entire simulated space, and a *systemic* concentration, including the entire body.

All these molecules, except iron, diffuse through space, modeled using the Alternating Direction Implicit (ADI) method with a periodic boundary condition to implement diffusion [13]. The rationale for periodic boundary conditions is that the simulation covers a small area amid a large infected area. Therefore, the concentration of molecules across the boundaries should be similar. The level of cytokines and chemokines (TNF, IL-6, IL-10, CCL4, CXCL2, TGF-β) decay with a half-life of one hour [14–20]. Hepcidin and transferrin (Tf, $TfFe$, and $TfFe_2$) levels are dynamically calculated based on the global levels of IL-6; this is described in detail below, as part of the description of iron metabolism.

The exchange of molecules between the serum and the simulated volume is modeled using Equation 2. In this equation, x_{system} is the molecule's systemic concentration (see terminology above), x is the local concentration, k_{turn} is the turnover rate, and t is the time-step length (2 min). If $x_{system} > x$ the molecule flows from the serum into the simulated volume, while, if $x_{system} < x$, it flows from the simulated volume to the serum, increasing the molecule's decay:

$$y = (x - x_{system}) \times e^{-k_{turn} \times t} - x_{system}. \tag{2}$$

For the cytokines, chemokines, siderophores (TAFC and TAFCBI), and lactoferrin (Lf, $LfFe$, $LfFe_2$), x_{system} is zero; therefore, these molecules are always flowing out of the simulated volume. For transferrin (Tf, $TfFe$, and $TfFe_2$) and hepcidin, x_{system} is calculated dynamically according to the global levels of IL-6 (more on this below). When an anti-TNF injection is modeled, the initial level (x_{system}) for anti-TNF is set, and then decays with a half-life of five days [21]. In that case, the systemic levels of anti-TNF determine the global and local levels of this antibody.

Cells

The most important host cells in the model are recruited mononuclear phagocytes, hereafter referred to as macrophages. Figure 2 offers a description of macrophage interactions and state changes. The default state of macrophages is resting. They get activated upon contact with hyphae, swelling conidia, or TNF. It should be noted that in Figure 2, there is an intermediate state between resting and active. That state, 'activating,' accounts for the time it takes for the activation process to be completed, likewise for 'inactivating.'

Active macrophages secrete TNF, IL-6, and IL-10 [22–24], and are able to kill hyphae [25], but do not secrete chemokines. Only after extra priming with TNF do they become chemokine secretors [26–28]. When macrophages interact with apoptotic neutrophils, IL-10, or TGF-β, they become inactive, sometimes referred to as M2c macrophages [29], and begin to secrete TGF-β. Neither resting nor inactive

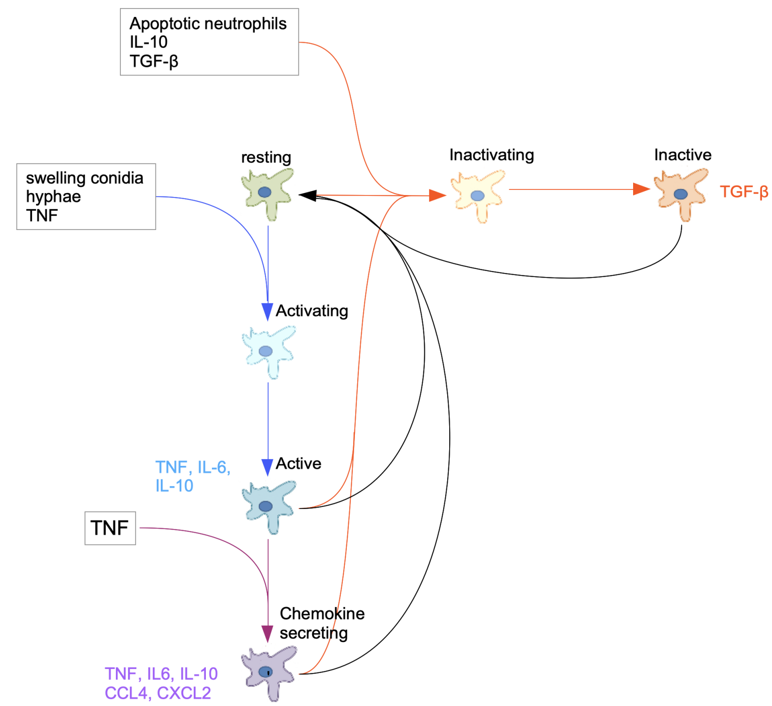

Fig 2. Figure showing macrophage state changes. By default, macrophages are resting. Swelling conidia, hyphae, or TNF cause them to transition to an activating (intermediate) state and then to the active state. Active macrophages secrete TNF, IL-6, and IL-10. Extra priming with TNF makes macrophages secrete chemokines as well (CCL4 and CXCL2). Apoptotic neutrophils, IL-10, or TGF-β, cause macrophages (including activated macrophages) to transition to an inactive TGF-β-secreting state. Active macrophages (blue and purple) can kill hyphae while resting, whereas inactive ones cannot. All macrophages return to a resting state after 6 hours (180 iterations) in the absence of a continuous stimulus.

macrophages can kill hyphae. In the absence of continuous stimuli, active and inactive macrophages eventually return to the resting state. See Table S1 in the supplementary materials for the numerical values of all model parameters.

Pneumocytes (type II pneumocytes) and neutrophils are intially in a resting state and get activated just like macrophages, but they do not have an inactive phenotype ("M2c") nor do they secrete IL-10. Pneumocytes can only interact with conidia and hyphae without killing them, while neutrophils can kill both, independent of their activation status. Active neutrophils secrete lactoferrin and small amounts of cytokines.

In the model, *Aspergillus fumigatus* has three life stages: resting conidia, swelling conidia, and hyphae. The hyphae are more or less continuous structures divided by septae [30]. Each of these subdivisions is a multinucleated cell-like structure, referred to as hyphal cells for simplicity.

In previous work, a dynamic gene regulatory network of iron uptake by *Aspergillus fumigatus* was developed [11], that is used here as a component model, with minor adjustments.

In simulations, *Aspergillus fumigatus* starts out as resting conidia; after 4 hours they start swelling with a half-life of 6 hours (see Table S1) - that is, half the conidia swell after 6h. Beyond that, it takes 2 hours until they become able to grow into hyphal cells. However, even after 2 hours, they will only grow if iron levels are adequate, as measured by the Boolean labile iron pool node LIP in the model; that is, growth is limited by iron.

Although hyphal growth is a continuous process, the model uses a discrete approximation. A tip cell can produce another tip cell (elongation), while a sub-tip cell can form a 45-degree branch (subapical branch) [30,31] with 25% probability. Other cells cannot originate new cells unless their neighbors are killed, and they become tip or sub-tip cells again. The interaction of swelling conidia with a macrophage or neutrophil leads to their phagocytosis and subsequent death. Both events have a certain probability of happening; see Table S1. The interaction of these leukocytes with a hyphal cell leads to its death with some probability (see Table S1). Resting conidia do not interact with immune cells.

Cell Movement

Cell movement can be divided into two modes: magnitude and direction. Magnitude is the number of voxels the cell will move. A Poisson random number generator is used to decide how many voxels it will move, based on its movement rate. In the absence of chemokines, cells drift randomly. When chemokines are present, each voxel receives a weight according to Equation 3:

$$w_i = 1 - e^{-\frac{x_i}{k_d}}. \tag{3}$$

where x_i is the chemokine concentration in neighboring voxel i, w_i is the corresponding weight of this voxel, and k_d is the chemokine dissociation constant.

The cell will then move to a neighboring voxel (v_i) with probability proportional to the voxel weight ($p_i \propto w_i$). Only macrophages and neutrophils move. The former are attracted by CCL4 and the latter by CXCL2.

Recruitment of cells

As with movement, only macrophages and neutrophils are recruited by CCL4 and CXCL2, respectively. Equation 4 is used to compute the average number of cells that will be recruited in the next iteration:

$$n = \frac{k_r \times X}{k_d} \times (1 - \frac{N}{K}), \tag{4}$$

where N is the current number of cells in the simulator, K is the carrying capacity, k_r is the global recruitment rate, k_d is the dissociation constant of the chemokine, X is the global amount of the chemokine, and the real number n is the average number of cells to be recruited. This number is used by a Poisson random number generator to decide how many cells will be recruited. Macrophages and neutrophils have half-lives of 24 and 6 hours, respectively [32,33]. The quantity of cells in the simulator is a balance between the number of cells recruited according to Equation 4 and the number of cells that die.

Iron metabolism

As mentioned before, the systemic levels of hepcidin and transferrin are computed dynamically, using the global level of IL-6. Equation 5 is used to compute how the systemic level of hepcidin change according to the global level of IL-6:

$$Log_{10}(Hepcidin_{systemic}) = hep_{int} + hep_{slope} \times Log_{10}(\frac{IL6_{global}}{2}). \tag{5}$$

This equation is based on data from Tabbah S *et al.* 2018 [34], correlating systemic levels of IL-6 to systemic levels of hepcidin. A reasonable estimate of the systemic levels of IL-6 is approximately 1/2 of the global level [35]. Therefore, one needs to divide $IL6_{global}$ by 2 in Equation 5. The hep_{int} and hep_{slope} in Equation 5 are parameters (intercept and slope). Equation 5 is only evaluated if $IL6_{global} > 1.37 \times 10^{-10}M$. To explain these thresholds, it should be noted that Equation 6 computes the systemic concentration of transferrin. Like the previous equation, this one is also "data-driven" [36]. The increase/decrease in systemic transferrin in Equation 6 refers to total transferrin. The proportions of Tf, $TfFe$, and $TfFe_2$ are unaffected, based on work that reports a low correlation between hepcidin and transferrin saturation [37]. See Table S1 for the proportions of Tf, $TfFe$, and $TfFe_2$.

$$Tf_{systemic} = Tf_{int} + Tf_{slope} \times Log_{10}(Hepcidin_{systemic}) \tag{6}$$

In Equation 6, Tf_{int} and Tf_{slope} are parameters (intercept and slope). Like with the previous equation, this equation is only evaluated if $Hepcidin_{systemic} > 10^{-8}M$. This threshold is consistent with the previous one used to evaluate Equation 5. The rationale for these thresholds is that these values generate a physiologic concentration of transferrin [38]. If the equation is evaluated below these values, transferrin may have an unrealistic concentration before and after infection.

Once systemic levels of hepcidin and transferrin are settled, their local concentrations tend asymptotically to these levels through Equation 2. Figure 3 describes the "battle over iron." TAFC and lactoferrin chelate iron bound to transferrin, decreasing the local levels of transferrin bound to iron ($TfFe$ and $TfFe_2$). TAFC is unable to "steal" iron from lactoferrin [39,40]. In parallel, hepcidin decreases transferrin levels, and it also acts on macrophages. The transfer of iron between molecules (TAFC, transferrin, and lactoferrin) is modeled by Michaelian kinetics (Equation 1). Both iron-binding sites in transferrin and lactoferrin are considered to have the same affinity, for simplicity, since cooperativity is not considered. The reaction is considered as unidirectional. Iron moves from transferrin to TAFC or lactoferrin, but not in the other direction.

Macrophages are continuously importing and exporting iron, maintaining a steady-state concentration under given physiological concentrations of transferrin. However, upon activation (contact with *A. fumigatus* or TNF) or hepcidin priming, macrophages lose their ability to export iron [41,42]. This loss, much like activation, is temporary, and in the absence of continuous stimuli, macrophages recover the ability to export iron.

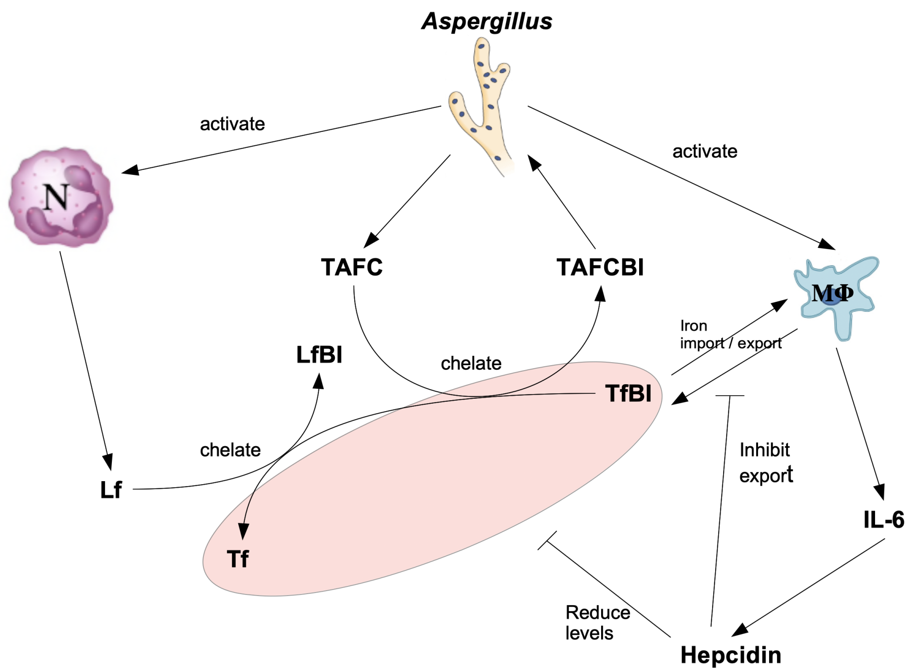

Fig 3. Figure showing the "battle over iron." *Aspergillus fumigatus* needs iron to survive and grow. It secretes siderophores (TAFC) that chelate iron from transferrin bound to iron ($TfBI = TfFe + TfFe_2$). Macrophages are continuously importing and exporting iron. Upon activation by *A. fumigatus*, they secrete IL-6. This cytokine induces the secretion of hepcidin by the liver. Hepcidin reduces transferrin levels (both free and bound to iron) and inhibits macrophage iron export. In parallel, upon contact with *A. fumigatus*, neutrophils secrete lactoferrin, which competes with TAFC for iron. Lactoferrin has 300 times more affinity for iron than transferrin. In the figure, Tf stands for transferrin, $TfBI$ for transferrin bound to iron ($TfFe$ and $TfFe_2$), Lf for lactoferrin, $LfBI$ lactoferrin bound to iron ($LfFe$ and $LfFe_2$), TAFC is the siderophore and TAFCBI the siderophore bound to iron.

Scaling from the simulated space to the whole lung

A pair of mouse lungs is assumed to have a volume of 1mL [43], containing 2.3×10^5 macrophages in the alveolar lumen [44] and 1×10^7 type-II alveolar epithelial cells [45]. The simulated space is $6.4 \times 10^{-2} \mu L$, thus containing 15 macrophages and 640 type-II epithelial cells initially. A high dose inoculum (10^7) is used for initialization. However, according to Pritchard, JN *et al.* 1985 [46], inoculated material distributes unevenly, with $\approx 1/3$ of the lung infected and the remainder clear. Since only one of the infected areas is simulated, the simulated space should have 1920 conidia. To scale neutrophils, one can also use the fact that infection is limited to $\approx 1/3$ of the lung. In other words, to convert the number of neutrophils and *Aspergillus* in the simulated space to the number in the whole lung (pair of lungs), one needs to multiply by 5028.

Calibration of the model

The strategy for model calibration is to obtain all the model parameters *a priori* (Supplementary Material) and then validate it using *de novo* experimental data. To capture some parameters, certain assumptions and surrogate mathematical models are needed (see the TAFC secretion rate in the supplementary material for an example). The model is calibrated to reproduce the dynamics at the alveolar lumen. That is, it was fit to the number of leukocytes (macrophages/monocytes and neutrophils) using data from bronchoalveolar lavage (BAL) [44].

Experimental methods

Neutrophil depletion and induction of aspergillosis.

All experiments were performed in accordance with the National Institutes of Health and Institutional Animal Care and Use Guidelines and were approved by the Animal Care and Use Committee of the University of Florida. Eight week-old male and female C57Bl/6 mice were purchased from the Jackson Laboratory and housed under specific pathogen-free conditions in the animal facilities of the University of Florida, and infected with Aspergillus as previously described by us [47]. Briefly, neutrophils were transiently depleted with an intraperitoneal injection of $400\mu g$ of anti-Ly6G antibody (clone 1A8, BioXcell) in 0.5ml saline. A cohort of mice received an equivalent amount of isotype control antibody (rat IgG2a, Clone 2A3, BioXcell), a day prior to intratracheal inoculation with *Aspergillus* conidia.

Flow Cytometry

Mouse lung flow cytometry was performed as described in [48]. Briefly, lungs were digested in a mixture of 200 $\mu g/mL$ DNaseI and 25 $\mu g/mL$ Liberase TM for 30 mins at 370 $^\circ C$. The digested lungs were serially passed through 70 and 40 μm filters to collect the single-cell suspension. After red blood cell lysis, cells were counted, and 1.5×10^6 cells were stained with a fixable APC Cy-7 conjugated live dead stain (Thermo Fisher) in PBS for 20 mins. After washing with FAC buffer, cells were incubated with anti-CD16/32 (Fc block, clone 93; eBioscience, San Diego, CA) and stained with PerCP-conjugated anti-CD45 (30-F11), FITC-conjugated anti-CD11b (M1/70), PE-conjugated CD64 (X54-5/7.1), PECy7-conjugated anti-CD11c (N418), V450-conjugated anti-MHCII (I-A/I-E), APC-conjugated anti-CD24 (M1/69), BV605-conjugated anti-Ly6g (1A8), BV711-conjugated Ly6c (HK 1.4), Texas Red -conjugated Siglec F (E50-2440). Flow cytometry data were acquired using 14 color BD Fortessa (BD Biosciences, San Jose, CA). 500,000 events /samples were acquired and analyzed with FlowJo software 9.0 (Tree Star Inc., Ashland, OR).

Bronchoalveolar lavage fluid cytokine measurement

BALF IL-6 and CXCL2 levels were measured using commercial ELISA kits (Invitrogen), as per manufacturers' instructions.

Results

This model was completely parameterized with data from the literature (supplementary material). For model validation, a set of papers is used that report time-series of critical variables present in the model, such as curves of neutrophils, TNF, IL6, and colony-forming units (CFU). These values are compared with those predicted by model simulation. These data are used to see if the model can reproduce the reported levels of the different variables and, most importantly, their timing. None of the papers selected for validation were used to calibrate the model.

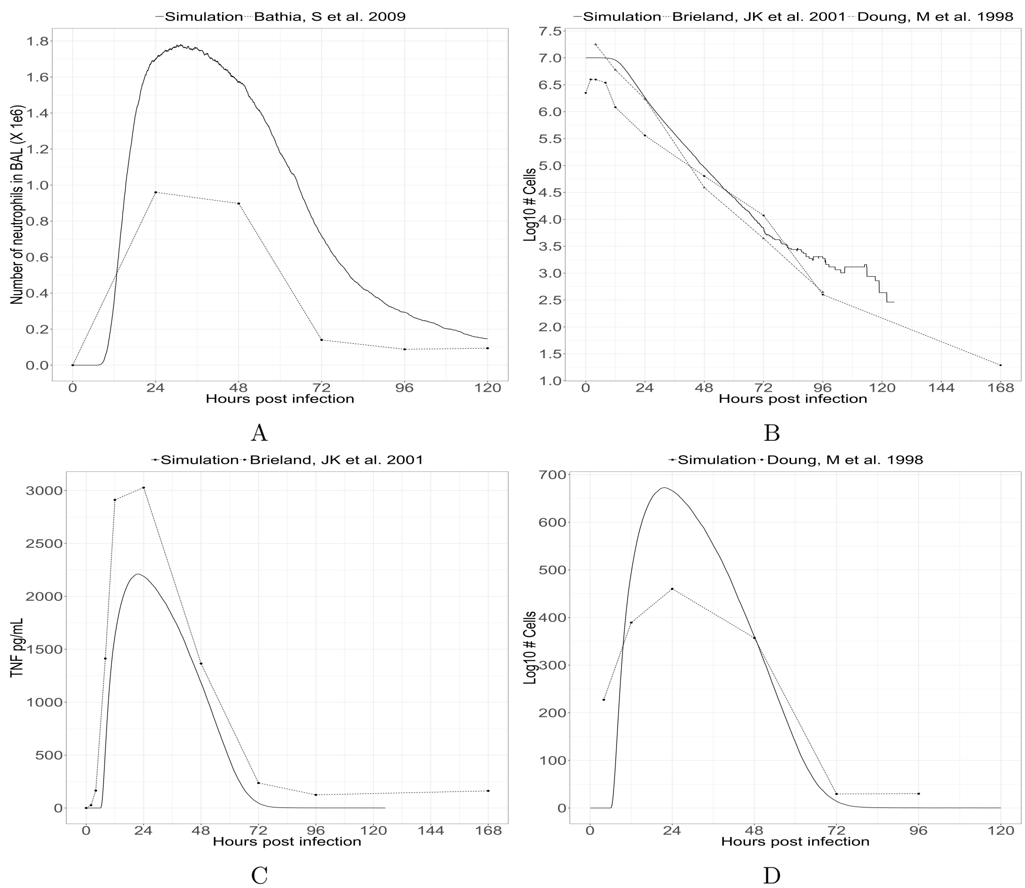

Fig 4. Figure showing the comparison of simulated data with data reported in the literature. To produce this figure, 36 simulations were performed, starting with an average of 1920 conidia, 15 macrophages, and 640 epithelial cells. Figure 4A: simulated time series of neutrophils and a time series reported by Bhatia, S *et al.* 2011 [49]. Figure 4B: simulated time series of conidia and time series reported by Brieland, JK et al. 2001 [50] and Doung, M *et al.* 1998 [51]. Figure 4C: simulated time series of TNF and time series reported by Brieland, JK *et al.* 2001 [50]. Figure 4D: simulated time series of IL-6 and time series reported by Doung, M *et al.* 1998 [51].

Figure 4 shows the comparison of simulation results with literature data. The simulator reproduces the correct levels of cells and cytokines and, most importantly, their timing. Figure 5 compares model outcomes with data generated by us. This figure shows a 72h time course of IL-6 and CXCL2 measured in BAL fluid and neutrophils and macrophages in lung homogenate. The model shows good agreement with the timing of these cells and molecules. As expected, whole lung cell suspensions contained greater numbers of leukocytes as compared to BAL [52,53], for which the model was calibrated. However, the simulator captures both the timing and the relative numbers of macrophages and neutrophils.

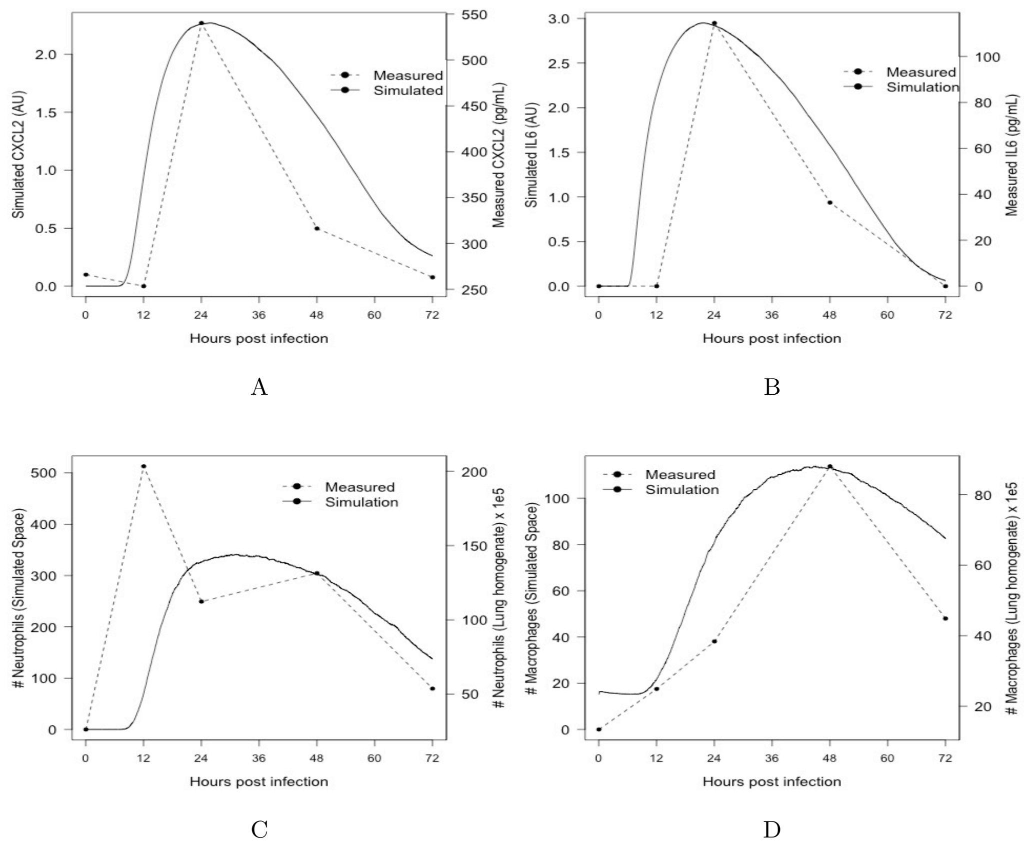

Fig 5. Figures showing the comparison of simulated data's timing with our experimental data. To produce this figure, 36 simulations were performed, starting with an average of 1920 conidia, 15 macrophages, and 640 epithelial cells. Figure 5A: comparison of simulated time series of CXCL2 with experimental data measured in BAL. Figure 5B: comparison of simulated time series of IL-6 with experimental data measured in BAL. Figure 5C: Comparing the number of neutrophils in simulated space with the number of neutrophils in lung homogenate. Figure 5D: Comparing the number of macrophages/monocytes in simulated space with the number of macrophages/monocytes in lung homogenate. Experimental data refer to mice infected with 7×10^6 conidia.

Biological data display a large degree of variability (see Figure 4D and 5B)), An extensive literature search was performed to compare the model to the available data. Table 1 present data from mice infected with 10^7 *Aspergillus fumigatus* conidia, measured 24h post-infection in BAL. This table includes neutrophils, CFU, IL-6, and TNF. The measures' average was computed, as well as the mean-squared error (MSE),

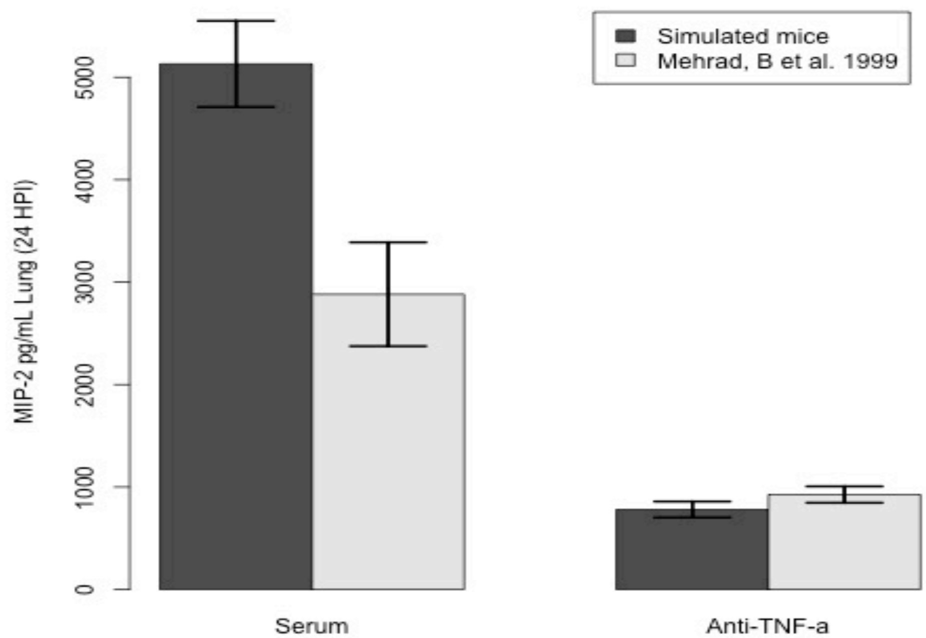

Fig 6. Figure showing the comparison of simulated data with data reported by Mehrad, B *et al.* 1999 [54]. Mice were injected serum or antibody (anti-TNF) concentration of 2×10^{-8} M, reaction rate 1.43×10^{6} $M * s^{-1}$ (1/Km), and half-life of 5 days, 24 before infection. To produce this figure, 36 simulations were performed, starting with an average of 1920 conidia, 15 macrophages, and 640 epithelial cells.

and the MSE between model prediction and data. The MSE standard deviation was calculated with bootstrap. It is noticeable that the model predictions are close to the measurement average (within one standard deviation), and the MSE's are also close (within one standard deviation). That means that the variability between simulated data and literature-reported data is within the variability among literature-reported data.

It is shown (Figure 4) that the model qualitatively reproduces cell numbers and cytokine concentrations over time reported in the literature. In particular, the fact that the model matches the temporal dynamics of these quantities is remarkable, given that it is a stochastic rule-based model, evolving in discrete time steps. Likewise, Figure 6 shows that the model correctly reproduces the drop in CXCL2 after an injection of anti-TNF antibody. In Figures 4 and 6, model predictions are only compared with a handful of published results. To show that this agreement is not due to a "selection bias," a larger collection of published data was incorporated, see Table 1, covering different experimental conditions, and cell numbers and cytokine levels 24 hours post-infection were compared with model predictions. The outcome is that the degree of disagreement between the model and the literature is similar to the disagreement among the different data sets in the literature that were considered. When comparing the model predictions with experimental data generated by us, it was found that it reproduces well the timing of IL-6 and CXCL2 (Figure 5A-B). It is worth pointing out in particular that the level of IL-6 measured in Figure 5 is within the range reported in

Table 1. Table showing validation with extended literature. All the papers in this table report data in BAL upon 24 hours post-infection and inoculate mice with $\approx 10^7$ conidia. Column 1 shows the reference; column 2 reported measurements of TNF; column 3 IL-6; column 4 neutrophils; and column 5 log_{10} of CFU. To calculate the mean-squared-error (MSE), data were normalized using average and standard deviation in line 9 so that different dimensions had the same weight. Simulated vs. literature MSE was calculated against the whole reported data (lines 1-8) and not against the average (line 9). Within-literature MSE was calculated comparing the average (line 9) with the reported data (lines 1-8). MSE standard deviation was calculated with bootstrap.

Reference	TNF	IL-6	Neutrophils	$Log_{10}(CFU)$
Bhatia, S *et al.* 2011 [49]			$9.60 \pm 0.14 \times 10^5$	
Brieland, JK *et al.* 2001 [50]	$3027 \pm 194 pg/mL$			5.56 ± 0.10
Cenci, E *et al.* 2001 [55]	$1602 \pm 297 pg/mL$	$348 \pm 52 pg/mL$		
Dubourdeau, M *et al.* [56]	$923 \pm 174 pg/mL$	$64 \pm 18 pg/mL$		
Doung, M *et al.* 1998 [51]		$460 \pm 8 pg/mL$		6.24 ± 0.16
Gresnigt, MS *et al.* 2016 [57]		$364 \pm 47 pg/mL$	$5.42 \pm 1.64 \times 10^5$	
Hohl, TM *et al.* 2005 [58]			$2.30 \pm 0.92 \times 10^6$	
Teschner, D *et al.* 2019 [59]	$592 \pm 48 pg/mL$	1964 ± 313	$4.04 \pm 1.25 \times 10^5$	4.38 ± 0.38
Average ± std-dev	**1536 ± 1079 pg/mL**	**676 ± 748 pg/mL**	$\mathbf{1.05 \pm 0.87} \times 10^6$	**5.39 ± 0.94**
Simulator ± std-dev	**2189 ± 118 pg/mL**	**666 ± 36 pg/mL**	$\mathbf{1.70 \pm 0.08} \times 10^6$	**6.26 ± 0.04**
MSE	within-literature:	**0.83 ± 0.18**	literature vs. simulator:	**1.09 ± 0.28**

Table 1.

Figure 6 compares the predicted levels of CXCL2 in mice that received an injection of anti-TNF antibody 24h before infection. These computational experiments are based on an estimate of the concentration and the anti-TNF-TNF reaction rate as well as its half-life [21, 60, 61] (supplemental material). As can be seen, the model correctly captures the fall in CXCL2 following anti-TNF injection.

Sensitivity analysis

An important aspect of modeling is the ability to measure the impact of parameter changes on model dynamics, thereby elucidating mechanisms. This can be achieved by a sensitivity analysis (SA), a method that starts by sampling the parameters, typically using Latin Hypercube sampling (LHS) to obtain a matrix of N samples by M parameters where each column (parameter) is entirely independent of the others. Next, a target output value is chosen to correlate the parameters. After running one simulation one constructs a new N (simulations) by M+1 (M parameters plus the output value) matrix and the Partial Ranking Correlation Coefficient between the parameters and the output variable.

The mean number of *Aspergillus* (conidia and hyphal cells) was used as the output parameter. Simulations are run for 48h or are stopped if the number of *Aspergillus* cells (conidia and hyphal cells) exceeds 1×10^5. If the number of conidia exceeds this value, it is safe to assume that it would monotonically increase. If that is the case, measuring the average number of *Aspergillus* through the simulation and performing ranking correlation is equivalent to measuring the area under the *Aspergillus* curve and performing ranking correlation. Therefore, parameters are correlated with fungal burden. A set of parameters is chosen to test, aiming to minimize redundancy. For example, cytokine secretion rates and cytokine kd, that control the cytokines affinity, play similar roles in the model. Therefore, only the kd is selected.

As can be seen in Table 2, the model is sensitive to parameters related to leukocytes, particularly neutrophils (CXCL2 kd, TNF kd, neutrophil half-life, and probability of neutrophils killing hyphae). On the fungus side, the time to grow (inverse of growth rate) has a large negative correlation, which is expected. Interestingly, the probability of swelling also has a strong negative correlation. Swelling is the first step for germination but is also the time when fungal cells become visible to the immune system. Leukocyte

Table 2. Table showing the Sensitivity Analysis (SA) of critical model parameters. Latin Hypercube Sampling (LHS) and Partial Ranking Correlation Coefficient (PRCC) were used to produce this analysis. The number of samples is adjusted according to the number of parameters being evaluated. Column 1 contains the parameter, Column 2 its description, and Column 3 the PRCC (mean±standard error). To calculate the PRCC in Column 3, 485 samples with simulated immunocompetent mice were performed. The range of parameter variation is one order of magnitude, with the default in the center. That is, min=1/3 default; max=3.333 default. In bold are the parameters that are more than 1.96 standard deviations away from 0.

Parameter	Description	PRCC
D	Diffusion rate	-0.0030 ± 0.0484
PR_SWELL	Probability of resting conidia to swell	**-0.8130 ± 0.0168**
$ITER\_CHANGE$	Iterations for cells to change state	**0.5745 ± 0.0337**
$ITER\_REST$	Iterations cells stay active	**-0.1707 ± 0.0488**
$ITER\_GROW$	Iiterations to grow a new septae	**-0.3212 ± 0.0458**
PR_BRANCH	Branch probability	-0.0041 ± 0.0452
$TURNOVER\_RATE$	Turnover rate	0.0103 ± 0.0488
LAC_QTTY	Lactoferrin secretion rate	**-0.1063 ± 0.0437**
$TAFC\_UP$	TAFC uptake rate	**0.1495 ± 0.0442**
MOL_HALF_LIFE	Cytokines and chemokines half-lives	-0.0273 ± 0.0468
$KdIL6$	k_d of IL6	-0.0567 ± 0.0472
$KdIL10$	k_d of IL10	0.0948 ± 0.0495
$KdCCL4$	k_d of CCL4	**0.1089 ± 0.0464**
$KdCXCL2$	k_d of CXCL2	**0.4325 ± 0.0402**
$KdTNF$	k_d of TNF-α	**0.2570 ± 0.0467**
$KdTGF$	k_d of TGF-β	-0.0528 ± 0.0522
$KdHep$	k_d of Hepcidin	-0.0254 ± 0.0460
$KdLIP$	A. fumigatus sensibility to iron	0.0067 ± 0.0445
$IRON\_EXP\_RATE$	Macrophage iron export rate	0.0093 ± 0.0488
$MOVE\_RATE$	Leukocytes movement rate	**-0.6655 ± 0.0301**
PR_MA_PHAG	Macrophage phagocytosis probability	-0.0552 ± 0.0504
PR_N_PHAG	Neutrophil phagocytosis probability	-0.0402 ± 0.0502
PR_P_INT	*Aspergillus* to interaction probability	-0.0841 ± 0.0503
PR_N_HYPHAE	Neutrophils probability to kill hyphae	**-0.2473 ± 0.0466**
PR_MA_HYPHAE	Macrophages probability to kill hyphae	-0.0226 ± 0.0481
PR_KILL	Probability to kill internalized conidia	**-0.2142 ± 0.0458**
K_M_TAFC	Tf-TAFC Michaelis constant	-0.0244 ± 0.0471
K_M_LAC	Tf-Lactoferrin Michaelis constant	-0.0326 ± 0.0483
N_HALF_LIFE	Probability of neutrophil to die	**0.2646 ± 0.0432**
MA_HALF_LIFE	Probability of macrophage to die	0.0233 ± 0.0418
HEP_SLOPE	Slope of the function IL6-Hepcidin	0.0473 ± 0.0497
TF_SLOPE	Hepcidin-Transferrin function's slope	-0.0763 ± 0.0472

movement rates were also strongly correlated with infection control. The faster leukocytes move, the faster they can reach fungal cells. The TAFC uptake rate and lactoferrin secretion showed a small but significant inverse correlation. The sensitivity analysis results agree broadly with the body of knowledge about this infection. That includes the importance of neutrophils and TNF, siderophores, and lactoferrin.

Discussion

Understanding the innate immune response to pathogens is of the utmost importance for designing effective therapeutic interventions. With increasing resistance of pathogens to anti-microbial drugs, it is imperative to explore host-centric therapeutics. This is the motivation for the work presented here. The goal was to understand some of the primary components of the innate immune response to fungal pathogens. In order to limit the immense complexity of mechanisms involved the model is focused on an essential component of nutritional immunity, the "battle over iron" between the host and the fungus in the context of a respiratory infection. The component of the immune response considered here involves many players, ranging from immune and fungal cells to molecular species such as cytokines, iron, and chemokines. It integrates events at the intracellular, tissue, organ, and system levels, and is governed by several intertwined feedback loops that create complex dynamics.

Without a computational model that captures relevant biology and is parameterized in a way that makes it more broadly valid and credible, it would be challenging to understand the interplay between the different components and make predictions about the effect of various perturbations. This paper describes a model that satisfies these criteria and can serve as the basis for future investigations. It is one of the most comprehensive models of this infection, parameterized entirely with information from the literature, and is validated using experimental data specifically generated for this purpose. It is also shown that it is broadly valid by verifying that it reproduces a wide range of experimental data reported in the literature (and not used for model calibration). This approach is different from the commonly used method of fitting the model parameters to one or more time courses of experimental data.

As a further validation step, a sensitivity analysis was performed to investigate the effect of individual parameters on model dynamics. Table 2 shows that the model agrees with a wide range of known facts about this infection. The sensitivity of model dynamics to neutrophil levels agrees with that reported in the extensive literature on the subject; see, e.g., [44,52,54,62]. The same is true for the sensitivity to TNF [54] and CXCL cytokines (CXCL2, in the case of our model) [52]. The positive effect of TAFC was also expected, since Schrettl, M *et al.* 2004 [63] reported that the TAFC knockout *A. fumigatus* has its virulence completely attenuated. Likewise, lactoferrin's protective effect agrees with *in vitro* studies that show this molecule's fungistatic effect [39,64].

The faster leukocytes move, the more conidia and hyphae they can reach. The sensitivity analysis shows that this parameter is the second most important one for infection control. Previously published models have shown that the ability to locate fungal cells is critical to fighting the disease. Pollmacher, J & Figge, MT 2014 [8] has shown that an unknown chemotactic signal is crucial for directing macrophages to the infection site and control the early infection phase. Simultaneously, a past model from our group has shown that the distance at which macrophages can detect fungal cells is a critical parameter determining infection outcome [10]. Like movement rate, the higher the sensing distance, the more fungal cells can be reached by macrophages. It is consequently not a surprise that sensitivity analysis identifies the most important model parameters as directly related to the visibility of the fungus to the immune system. Swelling of conidia is the first step to germination, but it is also the time when the immune system mounts its attack on the fungus, based on literature that reports little reaction of macrophages upon contact with resting conidia [22,65].

The model has several limitations. It does not currently incorporate an explicit physiological rendering of the lung tissue covered by the model, and several of the model features are not sufficiently mechanistic for the purpose of studying spatial events like hemorrhage, an important process affecting infection outcome.

In summary, the model described here has two important characteristics: (1) broad validity due to calibration with experimentally derived parameters rather than data fitting, and (2) extensive validation showing that the model can reproduce a wide range of results reported in the literature, covering different experimental conditions, in addition to reproducing data collected through dedicated experiments. The two characteristics establish the model as a credible tool to serve as a virtual laboratory for the study of the innate immune response to *Aspergillus fumigatus* infection, and as a base model that can be expanded by adding additional features of the immune response to respiratory infections by fungi and other pathogens.

Conclusion

Without dynamic computational models as a key technology for a systems view of complex biological processes governing human health, it is difficult or impossible to rigorously design control interventions that mitigate disease. Data-driven models are challenging to build and validate because available data are sparse in most cases, compared to what is needed to obtain meaningful such models. Mechanistic models are particularly useful for this purpose, if they are validated across a broad range of experimental conditions. Often, models are calibrated by fitting to one or several experimentally measured time courses. For models with many parameters, this limits their validity across a range of initial conditions.

The model described in this paper captures many mechanisms of the immune response to fungal infections. By necessity, this requires a large number of variables and parameters. Data from several longitudinal experiments are available that could have been used for data fitting. Instead, literature mining was used to obtain values for all the parameters in the model, or data from which those values can be derived. Time courses of experimental data are then used for model validation instead. As a result, the models can recapitulate a wide range of data and conditions reported in the literature. Experiments specifically designed for model validation were carried out as well. Going forward, this model can now be used as a virtual laboratory for hypothesis generation, and can also form the basis for a more comprehensive expanded model that can also be used for other respiratory diseases involving the immune system.

Supporting information

S1 File. Contains supplementary information on many aspects of the model, model parameters, and simulation.

Acknowledgments

This work was supported by the following grants: NIH 1U01EB024501-01, NSF CBET-1750183, and NIH 1 R01AI135128-01. R.L. was also partially supported by NIH Grant 1R01GM127909-01, B.M. by American Heart Association Grant 18TPA34170486, and B.A. by NIH Grant NIH T90-DE021989.

References

1. Pappas ea P G. Invasive fungal infections among organ transplant recipients: results of the Transplant-Associated Infection Surveillance Network (TRANSNET). Clin Infect Dis. 2010;50:1101–11.

2. Lai C, Yu W. COVID-19 associated with pulmonary aspergillosis: A literature review. J Microbiol Immunol Infect. 2021;54(1):46–53. doi:10.1016/j.jmii.2020.09.004.

3. Neofytus ea D. Epidemiology, outcomes, and mortality predictors of invasive mold infections among transplant recipients: a 10-year, single-center experience. Transpl Infect Dis. 2013;15:233–242.

4. van der Linden ea J W. Aspergillosis due to voriconazole highly resistant Aspergillus fumigatus and recovery of genetically related resistant isolates from domiciles. Clin Infect Dis. 2013;57:513–520.

5. Denning ea D W. Global burden of chronic pulmonary aspergillosis as a sequel to pulmonary tuberculosis. Bull World Health Organ. 2011;89(12):864–72.

6. Ganz T. Iron and infection. Int J Hematol. 2018;107(1):7–15. doi:10.1007/s12185-017-2366-2.

7. Blatzer M, Latge J. Metal-homeostasis in the pathobiology of the opportunistic human fungal pathogen Aspergillus fumigatus. Curr Opin Microbiol. 2017;40:152–159. doi:10.1016/j.mib.2017.11.015.

8. Pollmächer J, Figge MT. Agent-based model of human alveoli predicts chemotactic signaling by epithelial cells during early Aspergillus fumigatus infection. PloS one. 2014;9(10):e111630.

9. Pollmächer J, Figge MT. Deciphering chemokine properties by a hybrid agent-based model of Aspergillus fumigatus infection in human alveoli. Frontiers in microbiology. 2015;6:503.

10. Oremland M, Michels KR, Bettina AM, Lawrence C, Mehrad B, Laubenbacher R. A computational model of invasive aspergillosis in the lung and the role of iron. BMC systems biology. 2016;10(1):1–14.

11. Brandon M, Howard B, Lawrence C, Laubenbacher R. Iron acquisition and oxidative stress response in Aspergillus fumigatus. BMC systems biology. 2015;9(1):19.

12. Castiglione F. In: Meyers RA, editor. Agent Based Modeling and Simulation, Introduction to. New York, NY: Springer New York; 2009. p. 197–200.

13. Chang MJ, Chow LC, Chang WS. Improved Alternating-Direction Implicit Method For Solving Transient Three-Dimensional Heat Diffusion Problems. Numerical Heat Transfer, Part B: Fundamentals. 1991;19(1):69–84. doi:10.1080/10407799108944957.

14. Huhn RD, Radwanski E, Gallo J, Affrime MB, Sabo R, Gonyo G, et al. Pharmacodynamics of subcutaneous recombinant human interleukin-10 in healthy volunteers. Clinical Pharmacology & Therapeutics. 1997;62(2):171–180. doi:https://doi.org/10.1016/S0009-9236(97)90065-5.

15. Zahn G, Greischel A. Pharmacokinetics of tumor necrosis factor alpha after intravenous administration in rats. Dose dependence and influence of tumor necrosis factor beta. Arzneimittelforschung. 1989;39(9):1180–1182.

16. Oliver J, Bland L, Oettinger C, Arduino M, McAllister S, Aguero S, et al. Cytokine kinetics in an in vitro whole blood model following an endotoxin challenge. Lymphokine Cytokine Res. 1993;12(2):115–120.

17. Kuribayashi T. Elimination half-lives of interleukin-6 and cytokine-induced neutrophil chemoattractant-1 synthesized in response to inflammatory stimulation in rats. Lab Anim Res. 2018;34:80–83. doi:https://doi.org/10.5625/lar.2018.34.2.80.

18. Castell JV, Geiger T, Gross V, Andus T, Walter E, Hirano T, et al. Plasma clearance, organ distribution and target cells of interleukin-6/hepatocyte-stimulating factor in the rat. European Journal of Biochemistry. 1988;177(2):357–361. doi:https://doi.org/10.1111/j.1432-1033.1988.tb14383.x.

19. Toft A, Falahati A, Steensberg A. Source and kinetics of interleukin-6 in humans during exercise demonstrated by a minimally invasive model. Eur J Appl Physiol. 2011;111:1351–1359. doi:https://doi.org/10.1007/s00421-010-1755-5.

20. Wakefield L, Winokur T, Hollands R, Christopherson K, Levinson A, Sporn M. Recombinant latent transforming growth factor beta 1 has a longer plasma half-life in rats than active transforming growth factor beta 1, and a different tissue distribution. The Journal of Clinical Investigation. 1990;86(6):1976–1984. doi:10.1172/JCI114932.

21. Vieira P, Rajewsky K. The half-lives of serum immunoglobulins in adult mice. European Journal of Immunology. 1988;18(2):313–316. doi:https://doi.org/10.1002/eji.1830180221.

22. Gersuk GM, Underhill DM, Zhu L, Marr KA. Dectin-1 and TLRs Permit Macrophages to Distinguish between Different Aspergillus fumigatus Cellular States. The Journal of Immunology. 2006;176(6):3717–3724. doi:10.4049/jimmunol.176.6.3717.

23. Werner JL, Metz AE, Horn D, Schoeb TR, Hewitt MM, Schwiebert LM, et al. Requisite Role for the Dectin-1 b-Glucan Receptor in Pulmonary Defense against Aspergillus fumigatus. The Journal of Immunology. 2009;182(8):4938–4946. doi:10.4049/jimmunol.0804250.

24. Margalit A, Kavanagh K. The innate immune response to Aspergillus fumigatus at the alveolar surface. FEMS Microbiology Reviews. 2015;39(5):670–687. doi:10.1093/femsre/fuv018.

25. Roilides E, Sein T, Holmes A, Chanock S, Blake C, Pizzo P, et al. Effects of macrophage colony-stimulating factor on antifungal activity of mononuclear phagocytes against Aspergillus fumigatus. J Infect Dis. 1995;172(4):1028–1034. doi:10.1093/infdis/172.4.1028. PMID: 7561176.

26. Park SJ, Burdick MD, Brix WK, Stoler MH, Askew DS, Strieter RM, et al. Neutropenia Enhances Lung Dendritic Cell Recruitment in Response to Aspergillus via a Cytokine-to-Chemokine Amplification Loop. The Journal of Immunology. 2010;185(10):6190–6197. doi:10.4049/jimmunol.1002064.

27. Ciesielski C, Andreakos E, Foxwell B, Feldmann M. TNFa-induced macrophage chemokine secretion is more dependent on NF-kB expression than lipopolysaccharides-induced macrophage chemokine secretion. European Journal of Immunology. 2002;32(7):2037–2045. doi:https://doi.org/10.1002/1521-4141(200207)32:7¡2037::AID-IMMU2037¿3.0.CO;2-I.

28. Thorley AJ, Ford PA, Giembycz MA, Goldstraw P, Young A, Tetley TD. Differential Regulation of Cytokine Release and Leukocyte Migration by Lipopolysaccharide-Stimulated Primary Human Lung Alveolar Type II Epithelial Cells and Macrophages. The Journal of Immunology. 2007;178(1):463–473. doi:10.4049/jimmunol.178.1.463.

29. Arango Duque G, Descoteaux A. Macrophage Cytokines: Involvement in Immunity and Infectious Diseases. Frontiers in Immunology. 2014;5:491. doi:10.3389/fimmu.2014.00491.

30. Maheshwari R. 1. In: Fungi Experimental Methods in Biology. CRC Press; 2005.

31. Riquelme M, Bartnicki-Garcia S. Key differences between lateral and apical branching in hyphae of Neurospora crassa. Fungal Genet Biol. 2004;41(9):842–851. doi:10.1016/j.fgb.2004.04.006. PMID: 15288020.

32. Patel A, Zhang Y, Fullerton J, Boelen L, Rongvaux A, Maini A, et al. The fate and lifespan of human monocyte subsets in steady state and systemic inflammation. The Journal of experimental medicine. 2017;214. doi:10.1084/jem.20170355.

33. Tak T, Tesselaar K, Pillay J, Borghans JA, Koenderman L. What's your age again? Determination of human neutrophil half-lives revisited. Journal of Leukocyte Biology. 2013;94(4):595–601. doi:https://doi.org/10.1189/jlb.1112571.

34. Tabbah S, Buhimschi C, Rodewald-Millen K, Pierson C, Bhandari V, Samuels P, et al. Hepcidin, an Iron Regulatory Hormone of Innate Immunity, is Differentially Expressed in Premature Fetuses with Early-Onset Neonatal Sepsis. Am J Perinatol. 2018;35(9):865–872. doi:10.1055/s-0038-1626711.

35. Goncalves SM, Lagrou K, Rodrigues CS, Campos CF, Bernal-Martinez L, Rodrigues F, et al. Evaluation of Bronchoalveolar Lavage Fluid Cytokines as Biomarkers for Invasive Pulmonary Aspergillosis in At-Risk Patients. Frontiers in Microbiology. 2017;8:2362. doi:10.3389/fmicb.2017.02362.

36. Moran-Lev H, Weisman Y, Cohen S, Deutsch V, Cipok M, Bondar E, et al. The interrelationship between hepcidin, vitamin D, and anemia in children with acute infectious disease. Pediatr Res. 2018;84(1):62–65. doi:10.1038/s41390-018-0005-0.

37. Ryan E, Ryan J, D RJ, Coughlan B, Tjalsma H, Swinkels D, et al. Correlates of Hepcidin and NTBI according to HFE Status in Patients Referred to a Liver Centre. Acta Haematol. 2015;133:155–161. doi:10.1159/000363490.

38. Parmar JH, Mendes P. A computational model to understand mouse iron physiology and disease. PLOS Computational Biology. 2019;15(1):1–28. doi:10.1371/journal.pcbi.1006680.

39. Zarember K, Sugui J, Chang Y, Kwon-Chung K, Gallin J. Human polymorphonuclear leukocytes inhibit Aspergillus fumigatus conidial growth by lactoferrin-mediated iron depletion. J Immunol. 2007;178(10):6367–6373. doi:10.4049/jimmunol.178.10.6367.

40. Gazendam R, van Hamme J, Tool A, Hoogenboezem M, van den Berg J, Prins J, et al. Human Neutrophils Use Different Mechanisms To Kill Aspergillus fumigatus Conidia and Hyphae: Evidence from Phagocyte Defects. J Immunol. 2016;196(3):1272–1283. doi:10.4049/jimmunol.1501811.

41. Kong W, Duan X, Shi Z, Chang Y. Iron metabolism in the mononuclear phagocyte system. Progress in Natural Science. 2008;18(10):1197 – 1202. doi:https://doi.org/10.1016/j.pnsc.2008.03.024.

42. Hentze M, Muckenthaler M, Andrews N. Balancing acts: molecular control of mammalian iron metabolism. Cell. 2004;117(3):285–297. doi:10.1016/s0092-8674(04)00343-5.

43. Irvin CG, Bates J. Measuring the lung function in the mouse: the challenge of size. Respiratory research. 2003;4(1). doi:10.1186/rr199.

44. Bonnett CR, Cornish EJ, Harmsen AG, Burritt JB. Early Neutrophil Recruitment and Aggregation in the Murine Lung Inhibit Germination of Aspergillus fumigatus Conidia. Infection and Immunity. 2006;74(12):6528–6539. doi:10.1128/IAI.00909-06.

45. Dzhuraev G, Rodriguez-Castillo J, Ruiz-Camp J, Salwig I, Szibor M, Vadasz I, et al. Estimation of absolute number of alveolar epithelial type 2 cells in mouse lungs: a comparison between stereology and flow cytometry. Journal of Microscopy. 2019;275:36–50. doi:https://doi.org/10.1111/jmi.12800.

46. Pritchard J, Holmes A, Evans J, Evans N, Evans R, Morgan A. The distribution of dust in the rat lung following administration by inhalation and by single intratracheal instillation. Environmental Research. 1985;36(2):268–297. doi:doi.org/10.1016/0013-9351(85)90025-8.

47. Cagnina ea R E. Neutrophil-derived TNF drives fungal acute lung injury in chronic granulomatous disease. J Infect Dis. 2021;doi: 10.1093/infdis/jiab188.

48. Barletta ea K E. Adenosine A(2B) receptor deficiency promotes host defenses against gram-negative bacterial pneumonia. Amer J Respir Crit Care Med. 2012;186(10:1044–50.

49. Bhatia S, Fei M, Yarlagadda M, Qi Z, Akira S, Saijo S, et al. Rapid host defense against Aspergillus fumigatus involves alveolar macrophages with a predominance of alternatively activated phenotype. PLoS One. 2011;6(1):e15943. doi:10.1371/journal.pone.0015943.

50. Brieland J, Jackson C, Menzel F, Loebenberg D, Cacciapuoti A, Halpern J, et al. Cytokine networking in lungs of immunocompetent mice in response to inhaled Aspergillus fumigatus. Infect Immun. 2001;69(3):1554–1560. doi:10.1128/IAI.69.3.1554-1560.2001.

51. Duong M, Ouellet N, Simard M, Bergeron Y, Olivier M, Bergeron M. Kinetic study of host defense and inflammatory response to Aspergillus fumigatus in steroid-induced immunosuppressed mice. J Infect Dis. 1998;178(5):1472–1482. doi:10.1086/314425.

52. Mehrad B, Strieter RM, Moore TA, Tsai WC, Lira SA, Standiford TJ. CXC Chemokine Receptor-2 Ligands Are Necessary Components of Neutrophil-Mediated Host Defense in Invasive Pulmonary Aspergillosis. The Journal of Immunology. 1999;163(11):6086–6094.

53. Mehrad B, Moore TA, Standiford TJ. Macrophage Inflammatory Protein-1α Is a Critical Mediator of Host Defense Against Invasive Pulmonary Aspergillosis in Neutropenic Hosts. The Journal of Immunology. 2000;165(2):962–968. doi:10.4049/jimmunol.165.2.962.

54. Mehrad B, Strieter R, Standiford T. Role of TNF-alpha in pulmonary host defense in murine invasive aspergillosis. J Immunol. 1999;162(3):1633–1640.

55. Cenci E, Mencacci A, Casagrande A, Mosci P, Bistoni F, Romani L. Impaired antifungal effector activity but not inflammatory cell recruitment in interleukin-6-deficient mice with invasive pulmonary aspergillosis. J Infect Dis. (2001;184(5):610–7. doi:10.1086/322793.

56. Dubourdeau M, Athman R, Balloy V, Philippe B, Sengmanivong L, Chignard M, et al. Interaction of Aspergillus fumigatus with the alveolar macrophage. Med Mycol. (2006;44:S213–S217. doi:10.1080/13693780600904900.

57. Gresnigt M, Rekiki A, Rasid O, Savers A, Jouvion G, Dannaoui E, et al. Reducing hypoxia and inflammation during invasive pulmonary aspergillosis by targeting the Interleukin-1 receptor. Sci Rep. 2016;6:26490. doi:10.1038/srep26490.

58. Hohl T, Van Epps H, Rivera A, Morgan L, Chen P, *et al* . Aspergillus fumigatus Triggers Inflammatory Responses by Stage-Specific b-Glucan Display. PLOS Pathogens. 2005;1(3):e30. doi:https://doi.org/10.1371/journal.ppat.0010030.

59. Teschner D, Cholaszczynska A, Ries F, Beckert H, Theobald M, Grabbe S, et al. CD11b Regulates Fungal Outgrowth but Not Neutrophil Recruitment in a Mouse Model of Invasive Pulmonary Aspergillosis. Front Immunol. 2019;10:123. doi:10.3389/fimmu.2019.00123.

60. Goldbaum FA, Cauerhff A, Velikovsky CA, Llera AS, Riottot MM, Poljak RJ. Lack of Significant Differences in Association Rates and Affinities of Antibodies from Short-Term and Long-Term Responses to Hen Egg Lysozyme. The Journal of Immunology. 1999;162(10):6040–6045.

61. Colino J, Diez M, Outschoorn I. A quantitative ELISA for antigen-specific IgG subclasses using equivalence dilutions of anti-kappa and anti-subclass specific secondary reagents. Application to the study of the murine immune response against the capsular polysaccharide of Neisseria meningitidis serogroup B. J Immunol Methods. 1996;190(2):221–34. doi:10.1016/0022-1759(95)00278-2.

62. Schaffner A, Douglas H, Braude A. Selective protection against conidia by mononuclear and against mycelia by polymorphonuclear phagocytes in resistance to Aspergillus. Observations on these two lines of defense in vivo and in vitro with human and mouse phagocytes. J Clin Invest. 1982;69(3):617–631. doi:10.1172/jci110489.

63. Schrettl M, Bignell E, Kragl C, Joechl C, Rogers T, Arst J Herbert N, et al. Siderophore Biosynthesis But Not Reductive Iron Assimilation Is Essential for Aspergillus fumigatus Virulence. J Exp Med. 2004;200(9):1213–1219. doi:10.1084/jem.20041242.

64. Gazendam RP, van Hamme JL, Tool AT, Hoogenboezem M, van den Berg JM, Prins JM, et al. Human Neutrophils Use Different Mechanisms To Kill Aspergillus fumigatus Conidia and Hyphae: Evidence from Phagocyte Defects. The Journal of Immunology. 2016;196(3):1272–1283. doi:10.4049/jimmunol.1501811.

65. Chai L, Netea M, Sugui J, Vonk A, van de Sande W, Warris A, et al. Aspergillus fumigatus conidial melanin modulates host cytokine response. Immunobiology. 2010;215(11):915–920. doi:10.1016/j.imbio.2009.10.002.

The Innate Immune Response to Invasive Pulmonary Aspergillosis: A Systems Modeling Approach
Supplementary Material

Henrique AL Ribeiro, et al.

June 6, 2021

S1 The Parameters

Table S1: Table with the model parameters. Parameters 1-14 were obtained in a unified manner as described in the manuscript. As mentioned in the manuscript, "macrophage" should be interpreted as "macrophage/monocyte." Probabilities of phagocytosis, killing, and interaction refer to the likelihood of an event succeeding in one iteration if the appropriate conditions apply. The maximum number of cells and the average number of epithelial cells refer to the cells' quantity in the whole simulated space.

Id	Parameter	Description	Value	Reference
1	MA_IL6_QTTY	Macrophage/monocyte IL6 secretion rate.	1.46×10^{-20} $mol * cell^{-1} * h^{-1}$	[1, 2, 3, 4, 5, 6, 7, 8, 9, 10, 11, 12, 13, 14, 15, 16, 17, 18, 19, 20, 21, 22, 23, 24, 25, 26, 27, 28, 29, 30]
2	MA_CCL4_QTTY	Macrophage/monocyte CCL4 secretion rate	1.79×10^{-20} $mol * cell^{-1} * h^{-1}$	
3	MA_CXCL2_QTTY	Macrophage/monocyte CXCL2 secretion rate.	1.11×10^{-19} $mol * cell^{-1} * h^{-1}$	
4	MA_IL10_QTTY	Macrophage/monocyte IL10 secretion rate.	6.97×10^{-22} $mol * cell^{-1} * h^{-1}$	
5	MA_TNF_QTTY	Macrophage/monocyte TNF secretion rate.	3.22×10^{-20} $mol * cell^{-1} * h^{-1}$	
6	MA_TGF_QTTY	Macrophage/monocyte $TGF-\beta$ secretion rate.	1.01×10^{-21} $mol * cell^{-1} * h^{-1}$	
7	N_IL6_QTTY	Neutrophil IL6 secretion rate.	8.59×10^{-23} $mol * cell^{-1} * h^{-1}$	
8	N_CXCL2_QTTY	Neutrophil CXCL2 secretion rate.	6.50×10^{-22} $mol * cell^{-1} * h^{-1}$	
9	N_TNF_QTTY	Neutrophil TNF secretion rate.	1.89×10^{-22} $mol * cell^{-1} * h^{-1}$	
10	E_IL6_QTTY	Epithelial cells IL6 secretion rate.	1.46×10^{-20} $mol * cell^{-1} * h^{-1}$	
11	E_CCL4_QTTY	Epithelial cells CCL4 secretion rate	1.79×10^{-20} $mol * cell^{-1} * h^{-1}$	
12	E_CXCL2_QTTY	Epithelial cells CXCL2 secretion rate.	1.11×10^{-19} $mol * cell^{-1} * h^{-1}$	
13	E_TNF_QTTY	Epithelial cells TNF secretion rate.	3.22×10^{-20} $mol * cell^{-1} * h^{-1}$	
14	LAC_QTTY	Lactoferrin secretion rate (Neutrophils)	4.37×10^{-17} $mol * cell^{-1} * h^{-1}$	[31]
15	k_d_IL6	IL-6 k_d	330 pM	[32, 33, 34]
16	k_d_CCL4	CCL4 k_d	180 pM	[35]
17	k_d_CXCL2	CXCL2 k_d	91.667 pM	[36, 37]
18	k_d_IL10	IL-10 k_d	140 pM	[38, 39, 40, 41]
19	k_d_TNF	TNF k_d	326 pM	[42, 43, 44, 45, 46, 47, 48, 49]
20	$k_d\_TGF-\beta$	$TGF-\beta$ k_d	26.5 pM	[50, 51, 52]
21	k_d_HEP	Hepcidin k_d	855 nM	[53]
22	D	Diffusion rate	850 $\mu m^2/min$	[54, 55]

23	λ	Cytokines/chemokines half-life	1h	[56, 57, 58, 59, 60, 61, 62]
24	λ_{ab}	antibody half-life (Anti-TNF)	5 days	[63]
25	HEP_INT	Hepcidin intercept (IL6-hepcidin model)	-0.3141	[64]
26	HEP_SLOPE	Hepcidin slope (IL6-hepcidin model)	0.78	[64]
27	Tf_INT	Transferrin intercept (Tf-hepcidin model)	-1.194×10^{-5}	[65]
28	Tf_SLOPE	Transferrin slope (Tf-hepcidin model)	-5.523×10^{-6}	[65]
29	$Def\_TF\_CON.$	Default Tf concentration	32.25 μM	[66, 64, 65]
30	$APO\_Tf\_REL\_CON$	Apo-Tf relative concentration	40%	[66, 67]
31	$TfFe\_REL\_CON$	Monoferric Transferrin relative concentration	16.57%	
32	$TfFe2\_REL\_CON$	Diferric Transferrin relative concentration	43.43%	
33	MA_IRON_EXP	Macrophage iron export rate	2.13×10^{13}	[68]
34	MA_IRON_IMP	Macrophage iron uptake rate	0.083 $L * cell^{-1} * h^{-1}$	[68]
35	MA_INT_IRON	Macrophage initial internal iron quantity	$1.0086 \times 10^{-14} mol$	[66]
36	$TAFC\_QTTY$	TAFC secretion rate.	1.0×10^{-15} $mol * cell^{-1} * h^{-1}$	[69]
37	$TAFCBI\_UPTAKE$	TAFCBI (Bound to Iron) uptake rate	0.0156 $L * cell^{-1} * h^{-1}$	[70, 71]
38	$k_d\_Af\_IRON$	*A. fumigatus* iron sensibility	79.05 μM	[72]
39	K_M_TAFC	K_M TAFC-Tf	2.514 mM	[69, 67]
40	K_M_LAC	K_M Lactoferrin-Tf.	2.505 mM	[31]
41	K_M_AB	K_M Antibody-Antigen	0.697 μM	[73]
42	AB_CON	Antibody systemic concentration upon injection	0.2 nM	[74]
43	r	*A. fumigatus* growth rate	40 $\mu m/h$	[75, 76, 77, 78]
44	$MOVE\_RATE$	Leukocytes move rate	1.44 $\mu m/min$	[79]
45	N_H_KILL	Neutrophils-hyphae killing probability	22.71%.	[80, 81, 82, 83]
46	MA_H_KILL	Macrophage hyphal killing probability.	9.85%	[84, 85]
47	MA_PHAG	Macrophage phagocytosis probability	90.55%	[86, 87]
48	N_PHAG	Neutrophils phagocytosis probability	14.73%	[83]
49	$MA\_MAX\_CONIDIA$	Max ingested conidia by macrophage	18	[87]
50	$N\_MAX\_CONIDIA$	Max ingested conidia by neutrophils	3	[87, 88]
51	E_INT	Resting Epithelial cell-*Aspergillus* interaction probability	4.49%	[89]
52	$PHAG\_KILL$	Probability to kill internalized conidia (Leukocytes)	1.28%	[90]
53	MA_HALF_LIFE	Macrophage/monocytes half-life	24h	[91]
54	N_HALF_LIFE	Neutrophils half-life	6h	[92]

55	*SEPTAE_r*	septae radius	2.65 μm	[93, 94, 95]
56	*SEPTAE_L*	septae length	40 μm	[95, 96]
57	*T_SWELL*	Time to start swelling	4h	[97]
58	*PR_SWELL*	swelling probability	0.39%	[77, 98]
59	*T_GERM*	Time until germinating (after swelling)	2h	[97]
60	*T_CHANGE*	Iterations to cells change state	60	[99]
61	*T_REST*	Iterations to active cells return to resting	180	[99]
62	*H_VOL*	Hyphae volume	1.06 pL	[93, 94, 95, 96]
63	*MA_VOL*	Macrophages volume	4.85 pL	[100]
64	*CONIDIA_VOL*	Conidia volume	0.0484 pL	[94]
65	*PR_BRANCH*	probability of branching (*A. fumigatus*)	25%	[101, 75]
66	*TURNOVER_RATE*	Molecule exchange rate between lung and whole body serum.	0.1823 h^{-1}	[102]
67	*MAX_N*	Maximum number of neutrophils	522	[103]
68	*MIN_N*	Minimum number of neutrophils	0	[104]
69	*MAX_MA*	Maximum number of macrophages	209	[103]
70	*MIN_MA*	Minimum number of macrophages	15	[104]
71	*AVG_E*	Average number of epithelial cells	640	[105]
74	*REC_RATE*	Global recruitment rate	2	[104]
75	*Af_INIT_IRON*	*A. fumigatus* initial iron.	$3.83 \times 10^{-18} mol$	[94, 72]

S2 Parameter Acquisition

The model parameters are described in Table S1. In some cases, acquiring these values involved modeling, simplification, and some assumptions. In some cases, use was made of the MATLAB App Grabit. With this App, one can extract values directly from graphs and pictures. In cases, where more than one measurement is available, the value reported is the median.

S2.1 Cytokine and chemokine secretion rate

The selection of these rates was done using a collection of papers that report the secretion of cytokines in response to $\beta - glucan$, *A. fumigatus*, and, in some cases, LPS as a positive control. Each of these papers reports levels of two or more cytokines after monocyte or macrophage exposure with the respective stimulus. Because only papers that reported at least two cytokines were used, it was possible to construct a network of relative secretion rates. For instance, notice that across experimental procedures, the level of IL-6 is about 45% the level of TNF, while the level of IL-10 is about 4.7% of the level of IL-6, and so on.

This procedure was adopted because not all papers, notably those with β-glucan, can be quantified. In other words, a response against β-glucan is qualitatively similar to a response against live *A. fumigatus*. However, it is not known which concentration of β-glucan corresponds to which dose of fungus. With this procedure, however, one can use any piece of data with the implication that one has to fit this network to the actual secretion rate. However, having the actual secretion rate for only a few or even one cytokine is enough.

For this purpose, some papers for neutrophils and epithelial cells were used that compare cytokine secretion in these cells with macrophages. Therefore, in the model, these cells are scaled versions of macrophages. Neutrophils secrete 5.9% of what macrophages secret, and epithelial cells secrete the same as macrophages. However, none of these cells secrete IL-10 and TGF-β.

The lactoferrin parameter was acquired independently, and it is a rough approximation based on the amount of the protein a neutrophil carries.

S2.2 TAFC secretion and uptake rates

To calculate the TAFC secretion rate, Equation S2.1 was used to model the experiment of Hissen, AHT *et al.* 2004 [69]. This equation is a surrogate model for our simulator. It models conidia swelling and then secreting TAFC:

$$\frac{d^2[TAFC]}{dt^2} + \gamma * \frac{d[TAFC]}{dt} = \gamma * \sigma * C_0. \tag{S2.1}$$

In Equation S2.1, γ is the swelling rate, C_0 is the concentration of conidia in the experiment, and σ is the TAFC secretion rate, the parameter to be estimated. The value of γ is known from the model (Table S1) and C_0 from the paper itself. The initial condition is such that TAFC(4) = 0. That is, TAFC is zero at four hours, which comes from Table S1, to be interpreted as conidia starting to swell at four hours. Figure S1 shows the fitting of Eq S2.1 to the experimental data of Hissen, AHT *et al.* 2004 [69]. It should be noted that only σ is being fitted, and it should also be noted that the best one can obtain from this experiment is an apparent secretion rate.

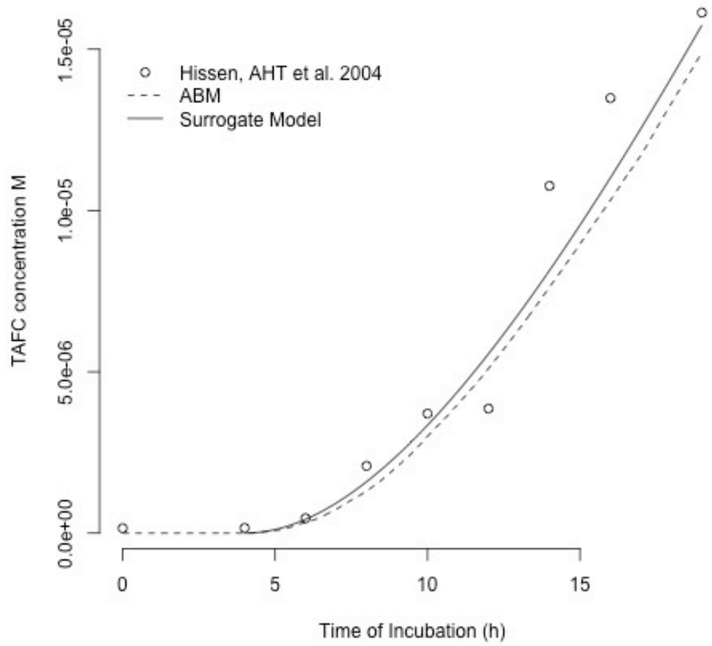

Figure S1: Figure showing the fitting of Eq S2.1. Experimental data from Hissen, AHT *et al.* 2004 [69] (represented as dots in the graph); computed with Eq S2.1 (solid line); computed with the data model (dashed line). Eq S2.1 was computed only from 4h onwards. Before that, we considered no swelling conidia and, therefore, no TAFC production (Table S1). The fact that the full simulator agrees with the surrogate model (Eq S2.1) shows that our procedure was appropriate.

To get the TAFC uptake rate, Raymond-Bouchard, I *et al.* 2012 [70] was used, who reports the TAFC uptake rate as OD600, and Yap, PY *et al.* 2019 [71] reports a curve of OD600 by yeast cell per mL. Supposing that *A. fumigatus* conidia OD600 is similar to that for yeast, one can calculate the TAFC uptake rate per *Aspergillus* cell.

As an approximation, it was assumed that a resting conidia contains one k_d (Section S2.6) of iron, therefore the *Aspergillus* initial amount of iron is $k_d\_Af\_IRON \times CONIDIA\_VOL$ (Table S1).

S2.3 Cytokine and chemokine k_d

The k_d of cytokines/chemokines is divided into two distinct sets of data: the k_d of cytokine/chemokine receptors and dose-response curves for these molecules. As an example of a dose-response curve, consider the level of activation of $NF - \kappa B$ vs. concentration of TNF. It was found that these two approaches are remarkably consistent; that is, activation of a cell by a molecule seems to depend, at least in general, only on the receptor affinity. To model dose-response curves, Equation 2 (Material & Methods) was used.

S2.4 Iron dynamics

The IL-6-hepcidin and hepcidin-Tf curves were obtained from the literature. While the macrophage iron import rate was also obtained from the literature, the export rate was assumed to be equal to the import rate. Homeostasis is assumed under normal conditions. Equality of iron import and export are interpreted to mean that the fluxes are equal, not the equations' constants. Iron import depends on external iron levels while export depends on internal iron levels.

Values for the internal concentration of macrophage iron, transferrin, and saturation are taken from Parmar, JH *et al.* 2019 [66].

S2.5 Phagocytosis, interaction, and killing rates

A simple law of mass action between leukocytes and conidia is assumed and used to derive an equation, (Eq S2.2). Given time and leukocyte concentration, this equation returns the probability of phagocytosing a conidium. The phagocytosis probability in Table S1 is an extrapolation of Eq S2.2 for a voxel's local concentration and one time step:

$$p = 1 - e^{-k*[L]*t} \tag{S2.2}$$

In Eq. S2.2, p is the probability of phagocytosis or interaction, 4[L]4 is the leukocyte concentration, and t is time, taken to be two minutes in the simulator (one time-step). Note that this extrapolation assumes that the limiting factor in the phagocytosis is the direct interaction between leukocyte and conidia and not the spread rate. According to Hoang, AN *et al.* 2013 [106], the leukocyte movement rate can be quite fast.

The hyphae killing rate is determined similarly. In contrast, the internalized conidia killing rate was acquired based on the percentage of internalized conidia killed by macrophages after 12h. Maximum conidia per macrophage is the apparent maximum reported by Gresnigt, MS *et al.* 2018 [87], and for neutrophils, it is a scaling of this number based on the relative size of a neutrophil.

S2.6 *Aspergillus* iron sensitivity

Aspergillus iron sensitivity ($k_d\_Af\_IRON$ in Table S1) is a critical parameter in the model. This value measures the concentration of iron needed to turn on/off the sreA gene. This gene, in turn, controls the secretion and uptake of TAFC [107]. As a simplification, this value is also used to control *Aspergillus* growth. Schrettl, M *et al.* 2008 [72] grew WT and sreA KO *Aspergillus* in the presence of TAFCBI (TAFC bound to iron) and then measured the content of iron as μ mol per gram of dry weight (DW) in the colonies.

The first thing to notice is that it is safe to assume that both colonies grew to approximately equal size based on Schrettl, M *et al.* 2008, and others. As mentioned, the paper measures iron in $\mu mol/g$ (DW). To convert this to molar, one can first convert DW into wet weight using data from Bakken, LR, 1983 [93]; this paper also gives the fungal density. With that one is able to calculate molarity.

The sreA KO cannot control the influx of TAFC. Therefore, one can assume, for simplicity, that the iron acquisition in these colonies follows a *quasi-linear* equation (Eq S2.3):

$$\frac{d[Fe_{KO}]}{dt} = k_{up} * h(t) * [TAFC], \tag{S2.3}$$

where k_{up} is the apparent TAFC uptake rate, $h(t)$ is the equation describing hyphal growth, and [TAFC] is the amount of TAFC in the experiment. This is assumed to be constant, that is, the quantity taken up by hyphae is small compared to the amount supplied. Integrating this equation, one gets:

$$[Fe_{KO}] = k_{up} * [TAFC] * \int h(t)dt \tag{S2.4}$$

This equation gives the quantity of internal iron at the end of the experiment with the sreA KO *Aspergillus*. For WT colonies, as iron concentration increases, sreA gets activated, which leads to the downregulation of the TAFC receptor. Therefore, for WT, one has:

$$\frac{d[Fe_{WT}]}{dt} = k_{up} * h(t) * [TAFC] * s([Fe_{WT}]) \tag{S2.5}$$

Here, $s([Fe_{WT}])$ is the unknown sreA activation function, but again, one can employ a surrogate model, namely Eq. 2 (Material & Methods) as a phenomenological model of sreA activation/inactivation. More specifically, this function is used to activate the LIP node that then inactivates the sreA node (see Brandon, M *et al.* 2015 [107]). The function $s([Fe_{WT}])$ should be the complement of that; therefore, Eq S2.5 becomes:

$$\frac{d[Fe_{WT}]}{dt} = k_{up} * h(t) * [TAFC] * e^{-\frac{[Fe_{WT}]}{k_d}}.$$

Integrating this equation one obtains:

$$\int e^{\frac{[Fe_{WT}]}{k_d}} d[Fe_{WT}] = k_{up} * [TAFC] * \int h(t)dt = [Fe_{KO}] + C,$$

where $C = k_d$. Making some algebraic rearrangements results in:

$$[Fe_{WT}] = k_d * \ln(\frac{[Fe_{KO}] + k_d}{k_d}),$$

where $[Fe_{WT}]$ is the quantity of iron in the WT experiment, $[Fe_{KO}]$ is the quantity of iron in the sreA KO experiment, and k_d is the value to be determined. The [TAFC] concentration is assumed to be high, compared to the amount consumed and that $h(t)$ is equal for sreA KO and WT.

S2.7 Transferrin Michaelis constant

For convenience, Michaelian kinetics is assumed. The TAFC-Tf kinetics is a complex mechanism described by Hissen, AHT & Moore MM 2005 [67] For convenience, a simplified version is used that does not consider cooperativity or difference in transferrin sites. The reaction rate of lactoferrin is very elusive, not having been studied extensively. Nevertheless, one study injected this protein *in vivo* and saw a 46% decrease in serum iron upon 4h [31]. That evidence enables an educated guess of the reaction rate.

Notice that when integrating these equations over the ABM, a time step of 2 minutes is used. The $Kcat$ ($Kcat^{app}$) is assumed to be 1 h^{-1}; therefore, one has to scale by 2/60 in the simulator. That is, in the simulator, one needs to choose an integration step of 2/60.

S2.8 Fungal biology

Fungal dimensions are obtained from the papers cited in Table S1. In some cases, values can be obtained directly from the photomicrograph reported in these papers using the MATLAB App Grabit. Growth rates come from papers that report hyphal length over time, while branching probability was based on the hyphal growth unit length. This gives an estimate of how many branches per septae there are.

A crucial parameter in the model is the swelling rate. Because swelling is quickly succeeded by germination, the germination rate is used as a proxy for the swelling rate. White, LO 1977 [98] report the rate of germination *in vivo*, and Gago, S *et al.* 2018 [77] report a very consistent value *in vitro* in the presence of bronchoepithelial cells. From these papers, one can make a robust estimate of this value.

S2.9 Number of cells and lung size

Calculations were made by considering a pair of inflated lungs, which has a volume of 1mL [108]. We consider that these pairs of lungs have around 3 million alveoli [109, 110], 230,000 resident macrophages [104], and ten million type-II epithelial cells [105]. The maximum number of mono and polymorphonuclear cells come from a paper reporting counts of these leukocytes per hundred alveoli in mice infected with *Aspergillus* [103]. The global recruitment rate was adjusted to fit the curve of neutrophils in Bonett, CR *et al.* 2006 [104]. Note that the numbers of macrophages and neutrophils reflect those of bronchoalveolar lavage fluid.

S2.10 Turnover rate

To calculate the turnover rate between the lung and the rest of the body, the following system of differential equations was used:

$$\begin{cases} \frac{dB}{dt} = b(t) - \lambda * B - k * (B - S) \\ \frac{dS}{dt} = k * (B - S) - \lambda * S, \end{cases}$$

where B is the concentration of the molecule in BAL, S is the concentration in serum, and λ is the decay rate. The function $b(t)$ is the secretion rate, and k is the exchange rate, the value to be estimated. The ratio of interest is B/S in the equilibrium. Notice that upon algebraic rearrangements, one finds that this ratio is $(k + \lambda)/k$. But λ is known from the literature (Table S1), and one can estimate k from an empirical B/S ratio found in Gonçalves, SM *et al.* 2017 [102].

S2.11 Leukocyte movement

This movement rate can be obtained from Khandoga, AG *et al.* 2009 [79]. The value, 1.44 $\mu m/min$, is conservative compared to other sources. Pollmacher J, & Figge MT, 2014 [111] uses a movement rate of 2-6 $\mu m/min$, for instance. Nevertheless, the rate used here must be considered a phenomenological movement rate. In the real lung, leukocytes may not move in a straight line but along the alveolar curved surface. That is the case in the Pollmacher J, & Figge MT, 2014 [111] model.

S2.12 Antibody

Antibody parameters were not specific for TNF. The concentration is obtained based on a measurement of IgG found in mice after an immunization assay. The value of Km resulted from the imposition of Michaelian kinetics, and on data for a generic protein antigen, in this case, the lysosome. Half-life comes from Vieira, P, and Rajewsky K 1988 [63].

S2.13 Other parameters

The time cells need to change status (T_CHANGE and T_REST) were based on *in-vitro* reports [99]. The half-life of molecules is an average. Likewise, the diffusion rate is an average of the values of the different molecules in living tissue.

For macrophages/monocytes, the 24h value reported for monocytes [91] is used. Other literature sources nevertheless report a longer half-life for macrophages. To calculate macrophages' volume, they can be approximated by a sphere, and one can then use the dimensions reported by Krombach, F *et al.* 1997 [100].

References

[1] Werner JL, Metz AE, Horn D, Schoeb TR, Hewitt MM, Schwiebert LM, et al. Requisite Role for the Dectin-1 b-Glucan Receptor in Pulmonary Defense against Aspergillus fumigatus. The Journal of Immunology. 2009;182(8):4938–4946. doi:10.4049/jimmunol.0804250.

[2] Taylor P, Tsoni S, Willment J, *et al* . Dectin-1 is required for β-glucan recognition and control of fungal infection. Nat Immunol. 2007;8:31–38. doi:https://doi.org/10.1038/ni1408.

[3] Gersuk GM, Underhill DM, Zhu L, Marr KA. Dectin-1 and TLRs Permit Macrophages to Distinguish between Different Aspergillus fumigatus Cellular States. The Journal of Immunology. 2006;176(6):3717–3724. doi:10.4049/jimmunol.176.6.3717.

[4] Hohl T, Van Epps H, Rivera A, Morgan L, Chen P, *et al* . Aspergillus fumigatus Triggers Inflammatory Responses by Stage-Specific b-Glucan Display. PLOS Pathogens. 2005;1(3):e30. doi:https://doi.org/10.1371/journal.ppat.0010030.

[5] Chai L, Netea M, Sugui J, Vonk A, van de Sande W, Warris A, et al. Aspergillus fumigatus conidial melanin modulates host cytokine response. Immunobiology. 2010;215(11):915–920. doi:10.1016/j.imbio.2009.10.002.

[6] Mark BH, Anthony JK, Christine CW. Inside the Neutrophil Phagosome: Oxidants, Myeloperoxidase, and Bacterial Killing. Blood. 1998;92(9):3007–3017. doi:https://doi.org/10.1182/blood.V92.9.3007.

[7] Celio GFdL, Xiao YQ, Shyra JG, Donna LB, William PS, Peter MH. Apoptotic Cells, through Transforming Growth Factor-β, Coordinately Induce Anti-inflammatory and Suppress Pro-inflammatory Eicosanoid and NO Synthesis in Murine Macrophages. J Biol Chem. 2006;281:38376–. doi:10.1074/jbc.M605146200.

[8] Fadok VA, Bratton DL, Konowal A, Freed PW, Westcott JY, Henson PM. Macrophages that have ingested apoptotic cells in vitro inhibit proinflammatory cytokine production through autocrine/paracrine mechanisms involving TGF-beta, PGE2, and PAF. The Journal of Clinical Investigation. 1998;101(2). doi:10.1172/JCI1112.

[9] Steele C, Rapaka R, Metz A, Pop S, Williams D, *et al* . The Beta-Glucan Receptor Dectin-1 Recognizes Specific Morphologies of Aspergillus fumigatus. PLOS Pathogens. 2005;1(4):e42. doi:doi.org/10.1371/journal.ppat.0010042.

[10] Adachi Y, Okazaki M, Ohno N, Yadomae T. Enhancement of cytokine production by macrophages stimulated with (1–¿3)-beta-D-glucan, grifolan (GRN), isolated from Grifola frondosa. Biol Pharm Bull. 1994;17(12):1554–1560. doi:10.1248/bpb.17.1554.

[11] Okazaki M, Adachi Y, Ohno N, Yadomae T. Structure-activity relationship of (1→3)-beta-D-glucans in the induction of cytokine production from macrophages, in vitro. Biol Pharm Bull 1995 Oct;18. 10;18(10):1320–7. doi:10.1248/bpb.18.1320.

[12] Brummer E, Kamberi M, Stevens DA. Regulation by Granulocyte-Macrophage Colony-Stimulating Factor and/or Steroids Given In Vivo of Proinflammatory Cytokine and Chemokine Production by Bronchoalveolar Macrophages in Response to Aspergillus Conidia. The Journal of Infectious Diseases,. 2003;187(4):705–709. doi:doi.org/10.1086/368383.

[13] Mihai GN, Warris A, Jos WMVdM, Matthew JF, Trees JGVJ, Liesbeth EHJ, et al. Aspergillus fumigatus Evades Immune Recognition during Germination through Loss of Toll-Like Receptor-4-Mediated Signal Transduction. The Journal of Infectious Diseases,. 2003;188(2):320–326. doi:doi.org/10.1086/376456.

[14] Marika K, Elmer B, Davidm AS. Regulation of Bronchoalveolar Macrophage Proinflammatory Cytokine Production By Dexamethasone and Granulocyte-Macrophage Colony-Stimulating Factor After Stimulation By Aspergillus Conidia Or Lipopolysaccharide. Cytokine,. 2002;19(1):14–20. doi:doi.org/10.1006/cyto.2002.1049.

[15] Warris A, Netea M, Verweij P, Gaustad P, Kullberg B, Weemaes C, et al. Cytokine responses and regulation of interferon-gamma release by human mononuclear cells to Aspergillus fumigatus and other filamentous fungi. Med Mycol. 2005;43(7):613–21. doi:10.1080/13693780500088333.

[16] Fadok VA, Bratton DL, Guthrie L, Henson PM. Differential Effects of Apoptotic Versus Lysed Cells on Macrophage Production of Cytokines: Role of Proteases. J Immunol. 2001;166(11):6847–6854. doi:10.4049/jimmunol.166.11.6847.

[17] Fujishima S, Hoffman AR, Vu KJ T Kim, Zheng H, Daniel D, Kim W Y, et al. Regulation of neutrophil interleukin 8 gene expression and protein secretion by LPS, TNF-α, and IL-1β. J Cell Physiol,. 1993;154:478–485. doi:10.1002/jcp.1041540305.

[18] Xing L, Remick D. Relative cytokine and cytokine inhibitor production by mononuclear cells and neutrophils. Shock. 2003;20(1):10–6. doi:10.1097/01.shk.0000065704.84144.a4.

[19] Altstaedt J, Kirchner H, Rink L. Cytokine production of neutrophils is limited to interleukin-8. Immunology,. 1996;89:563–568. doi:10.1046/j.1365-2567.1996.d01-784.x.

[20] Bondeson J, Browne K, Brennan F, Foxwell B, Feldmann M. Selective regulation of cytokine induction by adenoviral gene transfer of IkappaBalpha into human macrophages: lipopolysaccharide-induced, but not zymosan-induced, proinflammatory cytokines are inhibited, but IL-10 is nuclear factor-kappaB independent. J Immunol. 1999;162(5):2939–45.

[21] Abe Y, Hashimoto S, Horie T. Curcumin inhibition of inflammatory cytokine production by human peripheral blood monocytes and alveolar macrophages. Pharmacol Res. 1999;39(1):41–7. doi:10.1006/phrs.1998.0404.

[22] Loeffler J, Haddad Z, Bonin M, Romeike N, Mezger M, Schumacher U, et al. Interaction analyses of human monocytes co-cultured with different forms of Aspergillus fumigatus. Journal of Medical Microbiology. 2009;58(1):49–58. doi:doi.org/10.1099/jmm.0.003293-0.

[23] Simitsopoulou M, Roilides E, Likartsis C, Ioannidis J, Orfanou A, Paliogianni F, et al. Expression of Immunomodulatory Genes in Human Monocytes Induced by Voriconazole in the Presence of Aspergillus fumigatus. Antimicrobial Agents and Chemotherapy. 2007;51(3):1048–1054. doi:10.1128/AAC.01095-06.

[24] Lord PC, Wilmoth LM, Mizel SB, McCall CE. Expression of interleukin-1 alpha and beta genes by human blood polymorphonuclear leukocytes. The Journal of Clinical Investigation. 1991;87(4):1312–1321. doi:10.1172/JCI115134.

[25] Cassatella M. The production of cytokines by polymorphonuclear neutrophils. Immunol Today. 1995;16(1):21–6. doi:10.1016/0167-5699(95)80066-2.

[26] Ciesielski C, Andreakos E, Foxwell B, Feldmann M. TNFa-induced macrophage chemokine secretion is more dependent on NF-kB expression than lipopolysaccharides-induced macrophage chemokine secretion. European Journal of Immunology. 2002;32(7):2037–2045. doi:https://doi.org/10.1002/1521-4141(200207)32:7¡2037::AID-IMMU2037¿3.0.CO;2-I.

[27] Palmberg L, Larsson B, Malmberg P, Larsson K. Induction of IL-8 production in human alveolar macrophages and human bronchial epithelial cells in vitro by swine dust. Thorax. 1998;53(4):260–4. doi:10.1136/thx.53.4.260.

[28] Jablonski H, Rekasi H, Jager M. The influence of calcitonin gene-related peptide on markers of bone metabolism in MG-63 osteoblast-like cells co-cultured with THP-1 macrophage-like cells under virtually osteolytic conditions. BMC Musculoskelet Disord. 2016;17(199.). doi:doi.org/10.1186/s12891-016-1044-5.

[29] Katsuo K, Bo-Ram O. Optofluidic cellular immunofunctional analysis by localized surface plasmon resonance. Proc SPIE 9166, Biosensing and Nanomedicine VII, 91660R. 2014;doi:doi.org/10.1117/12.2062244.

[30] Thorley AJ, Ford PA, Giembycz MA, Goldstraw P, Young A, Tetley TD. Differential Regulation of Cytokine Release and Leukocyte Migration by Lipopolysaccharide-Stimulated Primary Human Lung Alveolar Type II Epithelial Cells and Macrophages. The Journal of Immunology. 2007;178(1):463–473. doi:10.4049/jimmunol.178.1.463.

[31] Jacques LvS, Pierre LM, Joseph FH. The Involvement Of Lactoferrin In The Hyposideremia Of Acute Inflammation. J Exp Med. 1974;140(4):1068–1084. doi. doi:https://doi.org/10.1084/jem.140.4.1068.

[32] Taga T, Hibi M, Hirata Y, Yamasaki K, Yasukawa K, Matsuda T, et al. Interleukin-6 triggers the association of its receptor with a possible signal transducer, gp130. Cell. 1989;58(3):573–81. doi:10.1016/0092-8674(89)90438-8.

[33] Gaillard J, Pugnière M, Tresca J, Mani J, Klein B, Brochier J. Interleukin-6 receptor signaling. II. Bio-availability of interleukin-6 in serum. Eur Cytokine Netw. 1999;10(3):337–44.

[34] Zohlnhöfer D, Graeve L, Rose-John S, Schooltink H, Dittrich E, Heinrich P. The hepatic interleukin-6 receptor. Down-regulation of the interleukin-6 binding subunit (gp80) by its ligand. FEBS Lett. 1992;306(2-3):219–22. doi:10.1016/0014-5793(92)81004-6.

[35] Samson M, LaRosa G, Libert F, Paindavoine P, Detheux M, Vassart G, et al. The second extracellular loop of CCR5 is the major determinant of ligand specificity. J Biol Chem. 1997;272(40):24934–24941. doi:10.1074/jbc.272.40.24934.

[36] Sai J, Fan GH, Wang D, Richmond A. The C-terminal domain LLKIL motif of CXCR2 is required for ligand-mediated polarization of early signals during chemotaxis. Journal of Cell Science. 2004;117(23):5489–5496. doi:10.1242/jcs.01398.

[37] Al-Alwan LA, Chang Y, Mogas A, Halayko AJ, Baglole CJ, Martin JG, et al. Differential Roles of CXCL2 and CXCL3 and Their Receptors in Regulating Normal and Asthmatic Airway Smooth Muscle Cell Migration. The Journal of Immunology. 2013;191(5):2731–2741. doi:10.4049/jimmunol.1203421.

[38] Liu Y, Wei S, Ho A, de Waal MR, Moore K. Expression cloning and characterization of a human IL-10 receptor. J Immunol. 1994;152(4):1821–9.

[39] Tan J, Indelicato S, Narula S, Zavodny P, Chou C. Characterization of interleukin-10 receptors on human and mouse cells. J Biol Chem. 1993;268(28):21053–21059.

[40] Ho AS, Liu Y, Khan TA, Hsu DH, Bazan JF, Moore KW. A receptor for interleukin 10 is related to interferon receptors. Proceedings of the National Academy of Sciences. 1993;90(23):11267–11271. doi:10.1073/pnas.90.23.11267.

[41] Carson W, Lindemann M, Baiocchi R, Linett M, Tan J, Chou C, et al. The functional characterization of interleukin-10 receptor expression on human natural killer cells. Blood. 1995;85(12):3577–85.

[42] Schall T, Lewis M, Koller K, Lee A, Rice G, Wong G, et al. Molecular cloning and expression of a receptor for human tumor necrosis factor. Cell. 1990;61(2):361–70. doi:10.1016/0092-8674(90)90816-w.

[43] Aggarwal B, Eessalu T, Hass P. Characterization of receptors for human tumour necrosis factor and their regulation by γ-interferon. Nature. 1985;318:665–667. doi:doi.org/10.1038/318665a0.

[44] Tsujimoto M, Yip YK, Vilcek J. Tumor necrosis factor: specific binding and internalization in sensitive and resistant cells. Proceedings of the National Academy of Sciences. 1985;82(22):7626–7630. doi:10.1073/pnas.82.22.7626.

[45] Baglioni C, McCandless S, Tavernier J, Fiers W. Binding of human tumor necrosis factor to high affinity receptors on HeLa and lymphoblastoid cells sensitive to growth inhibition. J Biol Chem. 1985;260(25):13395–7.

[46] Tsujimoto M, Vilcek J. Tumor Necrosis Factor-Induced Downregulation of Its Receptors in HeLa Cells. The Journal of Biochemistry,. 1987;102(6):1571–1577. doi:doi.org/10.1093/oxfordjournals.jbchem.a122206.

[47] Stauber G, Aiyer R, Aggarwal B. Human tumor necrosis factor-alpha receptor. Purification by immunoaffinity chromatography and initial characterization. J Biol Chem. 1988;263(35):19098–104.

[48] Hohmann H, Remy R, Brockhaus M, van Loon A. Two different cell types have different major receptors for human tumor necrosis factor (TNF alpha). J Biol Chem. 1989;264(25):14927–34.

[49] Ding A, Sanchez E, Srimal S, Nathan C. Macrophages rapidly internalize their tumor necrosis factor receptors in response to bacterial lipopolysaccharide. J Biol Chem. 1989;264(7):3924–9.

[50] Massague J, Like B. Cellular receptors for type beta transforming growth factor. Ligand binding and affinity labeling in human and rodent cell lines. J Biol Chem. 1985;260(5):2636–45.

[51] Kalter VG, Brody AR. Receptors for Transforming Growth Factor-β (TGF-β) on Rat Lung Fibroblasts Have Higher Affinity for TGF-β1 than for TGF-β2. American Journal of Respiratory Cell and Molecular Biology. 1991;4(5):397–407. doi:10.1165/ajrcmb/4.5.397.

[52] Wakefield L, Smith D, Masui T, Harris C, Sporn M. Distribution and modulation of the cellular receptor for transforming growth factor-beta. J Cell Biol. 1987;105(2):965–75. doi:10.1083/jcb.105.2.965. PMID: 2887577.

[53] Nemeth E, Tuttle MS, Powelson J, Vaughn MB, Donovan A, Ward DM, et al. Hepcidin Regulates Cellular Iron Efflux by Binding to Ferroportin and Inducing Its Internalization. Science. 2004;306(5704):2090–2093. doi:10.1126/science.1104742.

[54] Goodhill GJ. Diffusion in Axon Guidance. European Journal of Neuroscience. 1997;9:1414–1421. doi:10.1111/j.1460-9568.1997.tb01496.x.

[55] Goodhill G. Mathematical guidance for axons. Trends in Neurosciences. 1998;21(6):226–231. doi:10.1016/s0166-2236(97)01203-4.

[56] Huhn RD, Radwanski E, Gallo J, Affrime MB, Sabo R, Gonyo G, et al. Pharmacodynamics of subcutaneous recombinant human interleukin-10 in healthy volunteers. Clinical Pharmacology & Therapeutics. 1997;62(2):171–180. doi:https://doi.org/10.1016/S0009-9236(97)90065-5.

[57] Zahn G, Greischel A. Pharmacokinetics of tumor necrosis factor alpha after intravenous administration in rats. Dose dependence and influence of tumor necrosis factor beta. Arzneimittelforschung. 1989;39(9):1180–1182.

[58] Oliver J, Bland L, Oettinger C, Arduino M, McAllister S, Aguero S, et al. Cytokine kinetics in an in vitro whole blood model following an endotoxin challenge. Lymphokine Cytokine Res. 1993;12(2):115–120.

[59] Kuribayashi T. Elimination half-lives of interleukin-6 and cytokine-induced neutrophil chemoattractant-1 synthesized in response to inflammatory stimulation in rats. Lab Anim Res. 2018;34:80–83. doi:https://doi.org/10.5625/lar.2018.34.2.80.

[60] Castell JV, Geiger T, Gross V, Andus T, Walter E, Hirano T, et al. Plasma clearance, organ distribution and target cells of interleukin-6/hepatocyte-stimulating factor in the rat. European Journal of Biochemistry. 1988;177(2):357–361. doi:https://doi.org/10.1111/j.1432-1033.1988.tb14383.x.

[61] Toft A, Falahati A, Steensberg A. Source and kinetics of interleukin-6 in humans during exercise demonstrated by a minimally invasive model. Eur J Appl Physiol. 2011;111:1351–1359. doi:https://doi.org/10.1007/s00421-010-1755-5.

[62] Wakefield L, Winokur T, Hollands R, Christopherson K, Levinson A, Sporn M. Recombinant latent transforming growth factor beta 1 has a longer plasma half-life in rats than active transforming growth factor beta 1, and a different tissue distribution. The Journal of Clinical Investigation. 1990;86(6):1976–1984. doi:10.1172/JCI114932.

[63] Vieira P, Rajewsky K. The half-lives of serum immunoglobulins in adult mice. European Journal of Immunology. 1988;18(2):313–316. doi:https://doi.org/10.1002/eji.1830180221.

[64] Tabbah S, Buhimschi C, Rodewald-Millen K, Pierson C, Bhandari V, Samuels P, et al. Hepcidin, an Iron Regulatory Hormone of Innate Immunity, is Differentially Expressed in Premature Fetuses with Early-Onset Neonatal Sepsis. Am J Perinatol. 2018;35(9):865–872. doi:10.1055/s-0038-1626711.

[65] Moran-Lev H, Weisman Y, Cohen S, Deutsch V, Cipok M, Bondar E, et al. The interrelationship between hepcidin, vitamin D, and anemia in children with acute infectious disease. Pediatr Res. 2018;84(1):62–65. doi:10.1038/s41390-018-0005-0.

[66] Parmar JH, Mendes P. A computational model to understand mouse iron physiology and disease. PLOS Computational Biology. 2019;15(1):1–28. doi:10.1371/journal.pcbi.1006680.

[67] Hissen AHT, Moore MM. Site-specific rate constants for iron acquisition from transferrin by the Aspergillus fumigatus siderophores N',N",N"'-triacetylfusarinine C and ferricrocin. J Biol Inorg Chem 10, 211–220. 2005;10:211–220. doi:https://doi.org/10.1007/s00775-005-0630-z.

[68] Sarkar J, Seshadri V, Tripoulas N, Ketterer M, Fox P. Role of ceruloplasmin in macrophage iron efflux during hypoxia. J Biol Chem. 2003;278(45):44018–24. doi:10.1074/jbc.M304926200.

[69] Hissen AHT, Chow JMT, Pinto LJ, Moore MM. Survival of Aspergillus fumigatus in Serum Involves Removal of Iron from Transferrin: the Role of Siderophores. INFECTION AND IMMUNITY. 2004;72(3):1402–1408.

[70] Raymond-Bouchard I, Carroll CS, Nesbitt JR, Henry KA, Pinto LJ, Moinzadeh M, et al. Structural Requirements for the Activity of the MirB Ferrisiderophore Transporter of Aspergillus fumigatus. Eukaryotic Cell. 2012;11(11). doi:10.1128/EC.00159-12.

[71] Yap PY, Trau D. Direct Yeast Cell Count At OD600. Tip Biosystems Pte Ltd. 2019;2019.

[72] Schrettl M, Kim HS, Eisendle M, Kragl C, Nierman WC, Heinekamp T, et al. SreA-mediated iron regulation in Aspergillus fumigatus. Molecular Microbiology,. 2008;70:27–43. doi:10.1111/j.1365-2958.2008.06376.x.

[73] Goldbaum FA, Cauerhff A, Velikovsky CA, Llera AS, Riottot MM, Poljak RJ. Lack of Significant Differences in Association Rates and Affinities of Antibodies from Short-Term and Long-Term Responses to Hen Egg Lysozyme. The Journal of Immunology. 1999;162(10):6040–6045.

[74] Colino J, Diez M, Outschoorn I. A quantitative ELISA for antigen-specific IgG subclasses using equivalence dilutions of anti-kappa and anti-subclass specific secondary reagents. Application to the study of the murine immune response against the capsular polysaccharide of Neisseria meningitidis serogroup B. J Immunol Methods. 1996;190(2):221–34. doi:10.1016/0022-1759(95)00278-2.

[75] Bocking SP, Wiebe MG, Robson GD, Hansen K, Christiansen LH, Trinci APJ. Effect of branch frequency in Aspergillus oryzae on protein secretion and culture viscosity. Biotechnol Bioeng,. 1999;65:638–648. doi:10.1002/(SICI)1097-0290(19991220)65:6¡638::AID-BIT4¿3.0.CO;2-K.

[76] Escobar N, Ordonez S, Wösten H, Haas P, de Cock H, Haagsman H. Hide, Keep Quiet, and Keep Low: Properties That Make Aspergillus fumigatus a Successful Lung Pathogen. Front Microbiol. 2016;7:438. doi:10.3389/fmicb.2016.00438.

[77] Gago S, Overton NLD, Ben-Ghazzi Nt. Lung colonization by Aspergillus fumigatus is controlled by ZNF77. Nat Commun 9,. 2018;3835. doi:https://doi.org/10.1038/s41467-018-06148-7.

[78] Meletiadis J, Meis JFGM, Mouton JW, Verweij PE. Analysis of Growth Characteristics of Filamentous Fungi in Different Nutrient Media. Journal of Clinical Microbiology. 2001;39(2):478–484. doi:10.1128/JCM.39.2.478-484.2001.

[79] Khandoga A, Khandoga A, Reichel C, Bihari P, Rehberg M, *et al*. In Vivo Imaging and Quantitative Analysis of Leukocyte Directional Migration and Polarization in Inflamed Tissue. PLoS ONE. 2009;4(3):e4693. doi:10.1371/journal.pone.0004693.

[80] Zarember K, Sugui J, Chang Y, Kwon-Chung K, Gallin J. Human polymorphonuclear leukocytes inhibit Aspergillus fumigatus conidial growth by lactoferrin-mediated iron depletion. J Immunol. 2007;178(10):6367–6373. doi:10.4049/jimmunol.178.10.6367.

[81] Gazendam RP, van Hamme JL, Tool AT, Hoogenboezem M, van den Berg JM, Prins JM, et al. Human Neutrophils Use Different Mechanisms To Kill Aspergillus fumigatus Conidia and Hyphae: Evidence from Phagocyte Defects. The Journal of Immunology. 2016;196(3):1272–1283. doi:10.4049/jimmunol.1501811.

[82] Gazendam R, van de Geer A, van Hamme J, Tool A, van Rees D, Aarts C, et al. Impaired killing of Candida albicans by granulocytes mobilized for transfusion purposes: a role for granule components. Haematologica. 2016;101(5):587–96. doi:10.3324/haematol.2015.136630.

[83] Roilides E, Dimitriadou-Georgiadou A, Sein T, Kadiltsoglou I, Walsh T. Tumor necrosis factor alpha enhances antifungal activities of polymorphonuclear and mononuclear phagocytes against Aspergillus fumigatus. Infect Immun. 1998;66(12):5999–6003. doi:10.1128/IAI.66.12.5999-6003.1998.

[84] Roilides E, Sein T, Holmes A, Chanock S, Blake C, Pizzo P, et al. Effects of macrophage colony-stimulating factor on antifungal activity of mononuclear phagocytes against Aspergillus fumigatus. J Infect Dis. 1995;172(4):1028–1034. doi:10.1093/infdis/172.4.1028. PMID: 7561176.

[85] Roilides E, Holmes A, Blake C, Venzon D, Pizzo P, Walsh T. Antifungal activity of elutriated human monocytes against Aspergillus fumigatus hyphae: enhancement by granulocyte-macrophage colony-stimulating factor and interferon-gamma. J Infect Dis. 1994;170(4):894–9. doi:10.1093/infdis/170.4.894.

[86] Philippe B, Ibrahim-Granet O, Prévost M, Gougerot-Pocidalo M, Sanchez PM, Van der Meeren A, et al. Killing of Aspergillus fumigatus by alveolar macrophages is mediated by reactive oxidant intermediates. Infect Immun. 2003;71(6):3034–42. doi:10.1128/iai.71.6.3034-3042.2003.

[87] Gresnigt MS, Becke rKL, Leenders F, Alonso MF, Wang X, Meis JF, et al. Differential Kinetics of Aspergillus nidulans and Aspergillus fumigatus Phagocytosis. J Innate Immun. 2018;10:145–160. doi:10.1159/000484562.

[88] Niemiec M, De Samber B, Garrevoet J, Vergucht E, Vekemans B, De Rycke R, et al. Trace element landscape of resting and activated human neutrophils on the sub-micrometer level. Metallomics. 2015;7(6):996–1010. doi:10.1039/c4mt00346b.

[89] Clark HR, Powell AB, Simmons KA, Ayubi T, Kale SD. Endocytic Markers Associated with the Internalization and Processing of Aspergillus fumigatus Conidia by BEAS-2B Cells. mSphere. 2019;4(1):e00663–18. doi:10.1128/mSphere.00663-18.

[90] Wasylnka J, Hissen A, Wan A, Moore M. Intracellular and extracellular growth of Aspergillus fumigatus. Med Mycol. 2005;43:S27–S30. doi:10.1080/13693780400029247.

[91] Patel A, Zhang Y, Fullerton J, Boelen L, Rongvaux A, Maini A, et al. The fate and lifespan of human monocyte subsets in steady state and systemic inflammation. The Journal of experimental medicine. 2017;214. doi:10.1084/jem.20170355.

[92] Tak T, Tesselaar K, Pillay J, Borghans J, Koenderman L. What's your age again? Determination of human neutrophil half-lives revisited. J Leukoc Biol. 2013;94(4):595–601. doi:10.1189/jlb.1112571.

[93] Bakken L, Olsen R. Buoyant densities and dry-matter contents of microorganisms: conversion of a measured biovolume into biomass. Appl Environ Microbiol. 1983;45(4):1188–1195. doi:10.1128/AEM.45.4.1188-1195.1983.

[94] Sugui J, Kwon-Chung K, Juvvadi P, Latgé J, Steinbach W. Aspergillus fumigatus and related species. Cold Spring Harb Perspect Med. 2014;5(2):a019786. doi:10.1101/cshperspect.a019786.

[95] Ding Z, Li M, Sun F, Xi P, Sun L, Zhang L, et al. Mitogen-activated protein kinases are associated with the regulation of physiological traits and virulence in Fusarium oxysporum f. sp. cubense. PLoS One. 2015;10(4):e0122634. doi:10.1371/journal.pone.0122634.

[96] Renshaw H, Vargas-Muñiz J, Juvvadi P, Richards A, Waitt G, Soderblom E, et al. The tail domain of the Aspergillus fumigatus class V myosin MyoE orchestrates septal localization and hyphal growth. J Cell Sci. 2018;131(3):jcs205955. doi:10.1242/jcs.205955.

[97] Schrettl M, Bignell E, Kragl C, Sabiha Y, Loss O, Eisendle M, et al. Distinct roles for intra- and extracellular siderophores during Aspergillus fumigatus infection. PLoS Pathog. 2007;3(9):1195–207. doi:10.1371/journal.ppat.0030128.

[98] White LO. Germination of Aspergillus fumigatus conidia in the lungs of normal and cortisone-treated mice. Sabouraudia,. 1977;Volume 15, Issue 1,:37–41. doi:https://doi.org/10.1080/00362177785190071.

[99] Sharif O, Bolshakov VN, Raines S, *et al* . Transcriptional profiling of the LPS induced NF-κB response in macrophages. BMC Immunol. 2007;8(1.). doi:doi.org/10.1186/1471-2172-8-1.

[100] Fritz K, Silvia M, Anne-Marie A, Gerlach JT, Jürgen B, Martina D. Cell Size of Alveolar Macrophages: An Interspecies Comparison. Environmental Health Perspectives. 1997;105(5):1261–1263. doi:10.2307/3433544.

[101] Trinci APJ. The hyphal growth unit of wild type and spreading colonial mutants of Neurospora crassa. Archiv Mikrobiol. 1973;91:127–136. doi:doi.org/10.1007/BF00424756.

[102] Goncalves SM, Lagrou K, Rodrigues CS, Campos CF, Bernal-Martinez L, Rodrigues F, et al. Evaluation of Bronchoalveolar Lavage Fluid Cytokines as Biomarkers for Invasive Pulmonary Aspergillosis in At-Risk Patients. Frontiers in Microbiology. 2017;8:2362. doi:10.3389/fmicb.2017.02362.

[103] Morgenstern DE, Gifford MAC, Li LL, Doerschuk CM, Dinauer MC. Absence of Respiratory Burst in X-linked Chronic Granulomatous Disease Mice Leads to Abnormalities in Both Host Defense and Inflammatory Response to Aspergillus fumigatus. Journal of Experimental Medicine. 1997;185(2):207–218. doi:10.1084/jem.185.2.207.

[104] Bonnett CR, Cornish EJ, Harmsen AG, Burritt JB. Early Neutrophil Recruitment and Aggregation in the Murine Lung Inhibit Germination of Aspergillus fumigatus Conidia. Infection and Immunity. 2006;74(12):6528–6539. doi:10.1128/IAI.00909-06.

[105] Dzhuraev G, Rodriguez-Castillo J, Ruiz-Camp J, Salwig I, Szibor M, Vadasz I, et al. Estimation of absolute number of alveolar epithelial type 2 cells in mouse lungs: a comparison between stereology and flow cytometry. Journal of Microscopy. 2019;275:36–50. doi:https://doi.org/10.1111/jmi.12800.

[106] Anh NH, Caroline NJ, Dimisko L, Hamza B, Martel J, Kojic N, et al. Measuring neutrophil speed and directionality during chemotaxis, directly from a droplet of whole blood. TECHNOLOGY. 2013;01(01):49–57. doi:doi.org/10.1142/S2339547813500040.

[107] Brandon M, Howard B, Lawrence C, Laubenbacher R. Iron acquisition and oxidative stress response in Aspergillus fumigatus. BMC systems biology. 2015;9(1):19.

[108] Irvin CG, Bates J. Measuring the lung function in the mouse: the challenge of size. Respiratory research. 2003;4(1). doi:10.1186/rr199.

[109] Knust J, Ochs M, Gundersen HJG, Nyengaard JR. Stereological Estimates of Alveolar Number and Size and Capillary Length and Surface Area in Mice Lungs. Anat Rec,. 2009;292:113–122. doi:10.1002/ar.20747.

[110] Mercer RR, Russell ML, Crapo JD. Alveolar septal structure in different species. Journal of Applied Physiology. 1994;7(3):1060–1066. doi:10.1152/jappl.1994.77.3.1060.

[111] Pollmächer J, Figge MT. Agent-based model of human alveoli predicts chemotactic signaling by epithelial cells during early Aspergillus fumigatus infection. PloS one. 2014;9(10):e111630.